FLUID MECHANICS

1. Introduction

Fluid mechanics is both a descriptive sc ience of the phenomena that occur when fluids flow and a quantitative science showing how these phenomena may be described in mathematical terms and predicted when appropriate conditions are prescribed. To a practicing chemical technologist, fluid mechanics is an entire body of knowledge, theoretical and empirical, qualitative and quantitative, allowing analysis of the performance of complex plant equipment handling moving fluids. Before being in a position to calculate the details of a flow, one needs to understand the phenomena well enough to model the process properly. At times the technologist's needs are best satisfied by an empirical correlation; at other times the necessary skills consist largely of knowing how to apply the idealized mathematical solutions to a practical situation.

This article provides a summary of our current understanding of flow phenomena and their mathematical description and an introduction to advanced methods of computation and measurement. Fluid mechanical applications are widespread, extending over most fields of engineering and many applied sciences, but the present article will be focussed on the main needs of a chemical technologist, namely the design and operation of plant equipment and its interaction with the environment. More details on general and specific topics can be found in many widely available textbooks, handbooks, journals, etc (1–15).

2. Mathematical Description of Fluid Motion

2.1. Fundamental Concepts. Fluid materials differ from solid materials in that fluids are capable of unlimited deformation and will keep deforming, as long as they are subjected to shear stresses, while solids will normally deform only by a finite amount. In some instances, as during extrusion of very viscous or plastic materials, one may encounter both fluid-like and solid-like behavior. Although all materials consist of discrete particles, such as molecules and atoms, most fluid mechanical phenomena can be adequately described under the continuum hypothesis, which considers that the material properties of the fluid are not affected by the process of subdivision, thus allowing the definition of a fluid element as a material entity in the fluid having an infinitesimally small volume. This idealization allows one to define derivatives at a mathematical point. For example, the velocity vector at a point in the fluid is defined as

$$\vec{V} = \lim_{\delta t \to 0} \frac{\delta \vec{s}}{\delta t} = \frac{d\vec{s}}{dt} \tag{1}$$

where $\vec{s}$ is the position vector of a fluid element that occupies that point and t is time. The study of flow phenomena under the continuum hypothesis is only appropriate when the changes of interest occur over length scales much larger than molecular sizes or mean free paths between molecular collisions, so that material properties are actually averages over a large number of molecules.

There are cases, however, in which the continuum assumption breaks down, eg, in rarefied gases or in aerosols of submicrometer particles. Then one must resort to more general analytical models.

Fluid mechanics is an exact science, governed by three universal principles, which have been confirmed by experimentation and are accepted as valid. These are the law of the conservation of mass, including the law of conservation of individual species, electric charge, etc; the energy principle, or first law of Thermodynamics; and the momentum principle, ie, Newton's second law.

The above principles are expressed in the form of mathematical equations according to two general types of formulations, the integral and the differential ones. In the integral formulation, the principles are applied to a system, consisting always of the same fluid particles and possibly encompassing solid components as well. Due to the highly deformable nature of fluids, and the difficulty or impossibility of tracing the locations of all fluid elements at different times, the integral formulation is usually applied over a control volume, rather than a system. A control volume may contain different fluid elements at different times, and the application of the fundamental principles requires that one keeps track of fluid particles that enter or exit the control volume at any time instant. The integral formulation is not concerned with local variations of properties within the control volume, but only overall changes. In contrast, the differential formulation, which expresses the fundamental principles as differential equations valid at every location in the fluid, resolves local values of properties. To solve the differential equations, one requires proper initial and/or boundary conditions to be specified. The boundary conditions are usually easy to state, at least where the boundaries are fixed in position. These usually correspond to the physical requirement that there is a specified flow through, or stress at, the boundary. On solid walls, this condition requires that the velocity component of fluid particles normal to the wall must vanish (no penetration condition). On interfaces between different phases, one often expresses this boundary condition as a requirement that pressure-difference forces across the interface must balance surface tension forces. Real fluids, which exhibit viscosity (a resistance to continuous deformation), also obey the principle of continuity of velocity, which asserts that the velocity of a flowing fluid does not suffer discontinuous changes at interfaces with other fluids or solids. As applied to flow past a solid wall, it asserts that the fluid velocity relative to the wall decreases to zero as the wall is approached (no slip condition).

The complexity of a mathematical solution procedure can be significantly reduced with the use of simplifying approximations of the equations of motion. In classical inviscid hydrodynamics, solid surfaces serve to confine or deflect the flow (no penetration condition), but are assumed to offer no retardation to the fluid, which maintains its mainstream velocity, even vanishingly close to the surface. Although classical hydrodynamics is suitable for describing kinematic features of the flow, it fails completely in other key areas; its most notable failure is the incorrect prediction that a solid object immersed in a flow experiences no net drag force from the fluid (D'Alembert's paradox). The inclusion of the no slip condition provides a more accurate prediction of flow phenomena consistent with experimental observations. This statement serves to emphasize that fluid mechanics still depends significantly on experiment to

verify that a given mathematical or numerical solution does describe reality. This is particularly true when multiple solutions are possible. Another common type of simplifying approximation is to assume that the fluid is incompressible, which means that its volume does not change as a result of pressure changes. This assumption describes fairly well most flow phenomena in liquid flows as well as in gas flows with velocities that are small compared to the speed of sound. On the other hand, it fails to describe even qualitatively other important phenomena, such as wave propagation.

2.2. Integral Equations of Motion. Some problems in fluid mechanics can be solved to a sufficient degree of accuracy by examining only the overall balances of mass, momentum, and energy. In applying these balances, an appropriate control volume is established first and the rates of accumulation of the quantities within the volume are balanced against their rates of generation within the volume and their rates of transport through the control surface, which encloses the volume. In most cases, the volume of interest is fixed in space, as for example the space within a pipe or tank. In other cases, as in wave propagation, a moving control volume with an attached coordinate system is more appropriate. A control volume showing the unit vector normal outwards to the control surface and the flow velocity vector on the surface is sketched in Figure 1**a**, while the same control volume showing the surface force and its decomposition into normal and shear components is sketched in Figure 1**b**.

Conservation of Mass. The general equation for the conservation of mass of a chemical species with concentration (mass per unit volume) c_i is the scalar equation:

$$\underbrace{\frac{\partial}{\partial t_B} c_i dB}_{\text{rate of change in } B} + \underbrace{{}_S c_i V \cos\theta \, dS}_{\text{convective flux through } S} = \underbrace{-{}_S J_i dS}_{\text{diffusive flux through } S} + \underbrace{{}_B R_i dB}_{\substack{\text{production by} \\ \text{chemical reaction}}} \qquad (2)$$

where t is time, B is the control volume, S is the control surface, V is the magnitude of the velocity, θ is the angle between the velocity vector and the outward normal vector on a control surface element, J_i is the boundary flux through difusion and R_i is the rate of production of species i by chemical reaction.

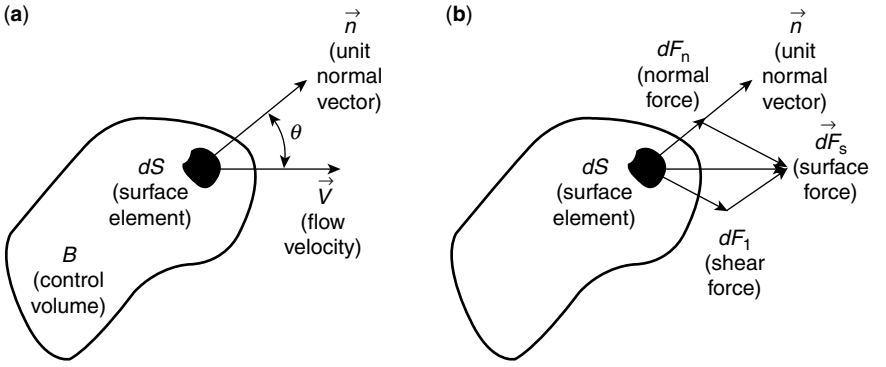

Fig. 1. Sketches of a typical control volume showing (**a**) the surface velocity and (**b**) the surface force.

Momentum Equation. The general equation for the balance of momentum is the vector equation:

$$\underbrace{\frac{\partial}{\partial t_B}\rho\vec{V}dB}_{\text{rate of change in } B} + \underbrace{{}_S\rho\vec{V}V\cos\theta dS}_{\text{convective flux through } S} = \underbrace{{}_B\vec{F}_B dS}_{\text{net body force}} + \underbrace{{}_S\vec{F}_S dB}_{\text{net surface force}} \tag{3}$$

where ρ is the fluid density. The two terms on the right-hand side represent the external forces applied on the control volume. The body forces arise from gravitational, electrostatic, and magnetic fields. The surface forces are the shear and normal forces acting on the fluid at its boundary; difusion of momentum, as manifested in viscosity, is included in these terms. In practice, the vector equation is usually resolved into its Cartesian components and the normal stresses are set equal to the pressures over those surfaces through which fluid is flowing.

Energy Equation. The specific (ie, per unit mass) energy of a flowing fluid is the sum of its internal, kinetic and potential specific energies:

$$e = u + \frac{V^2}{2} + gh \tag{4}$$

where h is the vertical elevation in the earth's gravitational field. The equation describing the conservation of energy, also expressing the first law of Thermodynamics, is the scalar equation:

$$\begin{aligned}\underbrace{\frac{\partial}{\partial t_B}\rho e dB}_{\text{rate of change in } B} &+ \underbrace{a_S\rho\left(e+\frac{P}{\rho}\right)V\cos\theta\, dS}_{\text{convective flux through } S} = \underbrace{Q}_{\substack{\text{heat transfer rate}\\ \text{from surroundings}}} \\ &- \underbrace{W_{sh}}_{\substack{\text{mechanical power by}\\ \text{shear stresses on S}}} - \underbrace{W_{other}}_{\substack{\text{electrochemical/radiation}\\ \text{power to surroundings}}}\end{aligned} \tag{5}$$

Note that the term containing the pressure P actually represents mechanical power by normal stresses on S, but has been grouped with the specific energy flux for convenience.

2.3. Differential Equations of Motion. The differential equations of motion can be derived from the corresponding integral ones, by letting the control volume vanish. These equations may be expressed in a coordinate system moving with the body (the Lagrangian viewpoint) or in a fixed coordinate system (the Eulerian viewpoint). In the following, we shall present the mass and momentum equations from the Eulerian viewpoint using a Cartesian coordinate system x_i, $i = 1,2,3$ and a control volume $dB = dx_1dx_2dx_3$. The velocity vector in this system is expressed as U_i, $i = 1,2,3$. The same equations in other coordinate systems and the differential energy equation are described in the general references mentioned above.

Conservation of Mass. Neglecting diffusion and chemical reactions, the differential mass conservation equation, also commonly referred to as the

continuity equation, is written as

$$\frac{\partial \rho}{\partial t} + \sum_{i=1}^{3} \frac{\partial (\rho U_i)}{\partial x_i} = 0 \tag{6}$$

For incompressible fluids, the density is constant and the continuity equation is simplified to

$$\sum_{i=1}^{3} \frac{\partial U_i}{\partial x_i} = 0 \tag{7}$$

Momentum Equation. This equation is derived by applying Newton's second law on an infinitesimal control volume, containing a fluid element. For a rigid body, this law states that the sum of external forces equals the product of its mass and its acceleration. In an Eulerian viewpoint formulation, the (total) acceleration of a fluid element is expressed as

$$\frac{DU_i}{Dt} = \frac{\partial U_i}{\delta t} + \sum_{j=1}^{3} U_j \frac{\partial U_i}{\partial x_j}, \quad i = 1, 2, 3 \tag{8}$$

in which the first term on the right-hand side is the local acceleration and the sum of the three other terms is the convective acceleration. The deformation rates of the fluid in different directions form the rate of strain tensor, expressed as

$$e_{ij} = \frac{1}{2}\left(\frac{\partial U_i}{\partial x_j} + \frac{\partial U_j}{\partial x_i}\right), \quad i, j = 1, 2, 3 \tag{9}$$

Next, it is necessary to understand the nature of the forces that might be exerted on this volume. There may be body forces, which, in Newtonian mechanics, are pictured as acting at a distance and include gravitational, electrostatic, and magnetic forces; if a noninertial frame of reference is used, one must also consider equivalent forces resulting from accelerations of the frame, eg, the centrifugal force. In addition, there are surface forces, exerted on the faces or edges of the element. Surface stresses arise from intermolecular forces and motions of molecules. At boundaries between phases, additional forces, which are generalizations of surface tension, must be included. Surface forces per unit surface area are called stresses. In the general case of an arbitrary surface element (Fig. 1**b**), one can define a normal stress and a shear stress as, respectively,

$$\sigma = \frac{dF_n}{dS} \quad \text{and} \quad \tau = \frac{\mathrm{dF_t}}{\mathrm{dS}} \tag{10}$$

When considering all stresses applied on an element with faces normal to the Cartesian axes and with all surface forces decomposed to their Cartesian

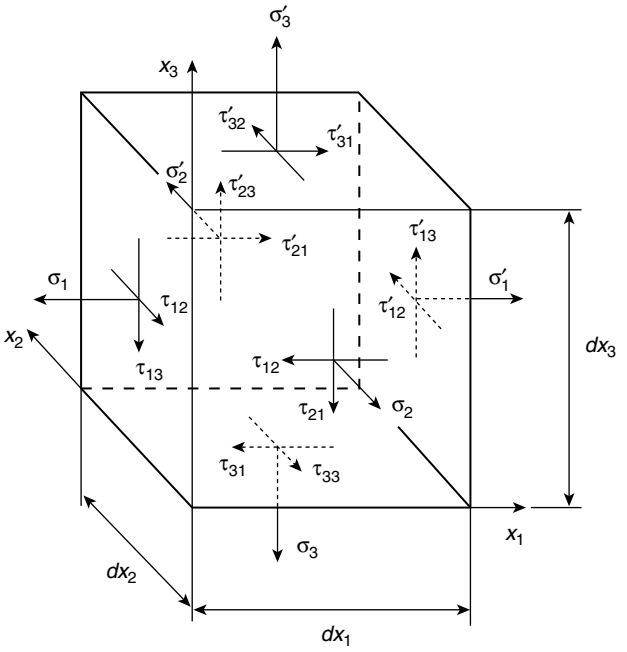

Fig. 2. Definition of stresses on a fluid element whose sides are aligned with the Cartesian axes. The positive directions of stresses are as indicated.

components, one would define stresses as the components of a symmetrical, second-order tensor (see Fig. 2)

$$\begin{bmatrix} \sigma_1 & \sigma_{12} & \tau_{13} \\ \tau_{21} & \sigma_2 & \tau_{23} \\ \tau_{31} & \tau_{32} & \sigma_3 \end{bmatrix} \tag{11}$$

In thermodynamics, pressure is defined as work by the fluid per unit volume. In fluid mechanics, pressure is defined as the average normal stress

$$P = -\frac{1}{3}(\sigma_1 + \sigma_2 + \sigma_3) \tag{12}$$

The negative sign is the result of the conventions that pressure is positive when compressive, while normal stresses are positive when tensile. In most cases, but not always, the fluid mechanical pressure may be taken as equal to the thermodynamic pressure. The variation of stresses along the Cartesian axes can be found by a Taylor series expansion, as, eg,

$$\sigma_1'(x_1 + dx_1) \approx \sigma_1(x_1) + \frac{\partial \sigma_1}{\partial x_1} dx_1 \tag{13}$$

Taking the above definitions into account, one may derive the differential momentum equation for a fluid element in Cartesian component form as

$$\rho\frac{DU_i}{Dt} = f_i + \frac{\partial\sigma_i}{\partial x_i} + \frac{\partial\tau_{ki}}{\partial x_k} + \frac{\partial\tau_{mi}}{\partial x_m}, \quad i = 1,2,3, \quad i \neq k \neq m \tag{14}$$

where f_i is the body force per unit volume.

Equation 14 gives the relation between stresses and acceleration obtained from momentum balance. The system of equations 6 (or 7) and 14 is not solvable, as it contains far too many unknowns. To proceed further, one needs to introduce appropriate constitutive equations, which codify the material properties through additional relations between the stresses and the rates of strain. The constitutive equations for a given fluid are found empirically or theoretically by use of some theory of material properties. The simplest model is one in which the various stresses are expressed as linear combinations of the rates of strain. When the fluid is homogeneous and isotropic, these relationships are simplified to ones that require only two material constants to be specified, the shear viscosity μ, and the dilatational viscosity λ. Further adopting the plausible condition $\lambda = 2/3\mu$, which is strictly valid only for incompressible fluids, one ends up expressing the stress–strain relationships using a single constant μ as

$$\sigma_i = -P + 2\mu\frac{\partial U_i}{\partial x_i} - \frac{2}{3}\mu\sum_{n=1}^{3}\frac{\partial U_n}{\partial x_n}, \quad i = 1,2,3 \tag{15}$$

$$\tau_{ij} = \tau_{ji} = \mu\left(\frac{\partial U_i}{j} + \frac{\partial U_j}{\partial x_i}\right), \quad i,j = 1,2,3, \quad i \neq j \tag{16}$$

Fluids that are described by such relationships are called Newtonian. The shear stresses are proportional to the viscosity, in accordance with experience and intuition. However, the normal stresses also have viscosity-dependent components, which is not an intuitively obvious result. For flow problems in which the viscosity is vanishingly small, the normal stress component is negligible, but for fluid of high viscosity, eg, polymer melts, it can be significant and even dominant. Substitution of these expressions into equations 14 leads to the Navier-Stokes (N-S) equations

$$\rho\frac{DU_i}{Dt} = f_i - \frac{\partial P}{\partial x_i} + \frac{\partial}{\partial x_i}\left[\mu\left(2\frac{\partial U_i}{\partial x_i} - \frac{2}{3}\sum_{n=1}^{3}\frac{\partial U_n}{\partial x_n}\right)\right] + \frac{\partial}{\partial x_k}\left[\mu\left(2\frac{\partial U_i}{\partial x_k} + \frac{\partial U_k}{\partial x_i}\right)\right] + \frac{\partial}{\partial x_m}\left[\mu\left(2\frac{\partial U_i}{\partial x_m} + \frac{\partial U_m}{\partial x_i}\right)\right], \quad i = 1,2,3, i \neq k \neq m \tag{17}$$

Further assuming that the viscosity is uniform in space, one gets the simplified and most commonly used N-S equation form

$$\rho\frac{DU_i}{Dt} = f_i - \frac{\partial P}{\partial x_i} + \mu\sum_{n=1}^{3}\frac{\partial^2 U_i}{\partial x_n^2}, \quad i = 1,2,3 \tag{18}$$

Equations 7 and 18 form a closed system of four equations with four unknowns, P and U_i, $i = 1,2,3$ (the body force, the density and the viscosity are assumed to be known by other means). Thus, given appropriate boundary and/or initial conditions, one may, at least in principle, solve these equations to compute the local velocity and pressure in incompressible Newtonian flows.

For some materials, the linear constitutive relation of Newtonian fluids is not accurate. Either stress depends on strain in a more complex way, or variables other than the instantaneous rate of strain must be taken into account. Such fluids are known collectively as non-Newtonian. Many different types of behavior have been observed, ranging from fluids for which the viscosity in the Navier-Stokes equation is a simple function of the shear rate to the so-called viscoelastic fluids, for which the constitutive equation is so different that the normal stresses can cause the fluid to flow in a manner opposite to that predicted for a Newtonian fluid.

There is actually a constitutive equation that is even simpler than that for the Newtonian fluid. This arises when internal fluid friction is neglected. Although this is not precisely true for a real fluid (the closest case would be liquid helium at temperatures <2 K), in many situations the flows calculated under this assumption are very close to those actually observed, at least in a significant portion of the flow field. Examples are high speed flows around obstacles in regions well away from solid boundaries or from wake regions. The importance of the frictionless flow theory lies in the wide variety of available solutions and in the powerful techniques of calculation available. When friction is neglected, the Navier-Stokes equations are simplified to the Euler equations

$$\rho \frac{DU_i}{Dt} = f_i - \frac{\partial P}{\partial x_i}, \quad i = 1, 2, 3 \tag{19}$$

which also form a closed system with the continuity equation 7.

By integrating the Euler equations along any streamline in the fluid and assuming that the body force is entirely gravitational, the flow is steady and the fluid is incompressible, one can derive the Bernoulli equation as

$$\frac{P}{\rho} + \frac{V^2}{2} + gh = \text{const along a streamline} \tag{20}$$

where h is the vertical elevation. One may actually derive Bernoulli's equation for the more general case of barotropic fluid (ie, one whose density is a function of pressure, as in the atmosphere and the oceans) to a form that replaces the pressure term by $(1/\rho)\, dP$. An unsteady form of Bernoulli's equation is also available. The value of the constant in equation 20 is generally different for different streamlines. Bernoulli's equation can provide the pressure as a function of velocity, making the solution of the momentum equation unnecessary. Continuity equation 7 alone cannot be solved for the velocity and additional assumptions are required. An assumption that is often made to simplify analysis of many problems in hydrodynamics and aerodynamics is that the flow is irrotational, namely, that its vorticity vector, defined as

$$\vec{\zeta} = curl \vec{V} \tag{21}$$

vanishes everywhere in the flow. Then, it becomes possible to define a scalar property, called the velocity potential, as

$$\phi = grad\vec{V} \tag{22}$$

and the continuity equation can be written as

$$\sum_{i=1}^{3} \frac{\partial^2 \phi}{\partial x_i^2} = 0 \tag{23}$$

Equation 23 is Laplace's equation, which also occurs in several other fields of mathematical physics, and can be solved analytically, numerically, and even graphically, much easier than the Navier-Stokes or Euler equations. An alternative approach for two-dimensional flow is to introduce a stream function ψ as

$$U_1 = \frac{\partial \psi}{\partial x_2}, \quad U_2 = -\frac{\partial \psi}{\partial x_1} \tag{24}$$

While the stream function automatically satisfies the two-dimensional, incompressible, continuity equation, the requirement that the flow is also irrotational leads to the equation

$$\sum_{i=1}^{2} \frac{\partial^2 \psi}{\partial x_i^2} = 0 \tag{25}$$

which is also Laplace's equation. Although the boundary conditions would differ, the approaches of using the velocity potential or the stream function to find the velocity of incompressible irrotational flows are mathematically equivalent.

2.4. Dimensional Analysis, Similarity and Modeling. The majority of technological flow problems are not solved by integrating the equations of motion. Instead, most are solved by carrying out laboratory experiments whose results are correlated, so as to yield useful information about systems that may differ greatly in size and in fluid properties. For the behavior of the experimental model to duplicate that of a system of interest, two criteria must, in principle, be met: first, the experimental apparatus must be geometrically similar to the system of interest; and second, certain dimensionless groupings of variables must be matched on the two systems. There are two basic methods available for determining the dimensionless groups appropriate to a given situation: dimensional analysis, which can be applied when the equations governing the process are not known; and similarity analysis, which proceeds from the governing equations and offers physical insights into the meanings of the groups.

Dimensional analysis is a mathematical technique that proceeds from the general principle that physical laws must be independent of the units of measurement used to express them. If one quantity is related to a group of other quantities, the quantities comprising the group must be related in such a manner that the net units or dimensions of the group are the same as those of the dependent quantity. A dimensionless group can then be formed immediately by

division. A useful tool, the Buckingham Pi theorem, asserts that the number of dimensionless groups needed to describe a situation is equal to the total number of variables less the number of fundamental dimensions needed to express them. Fundamental dimensions are generally taken to be length, time, mass, temperature, and heat content. The Pi theorem is a powerful tool because it limits the amount of experimental work needed to establish a general relationship. For example, consider the problem of determining the drag force F_D on a smooth sphere around which a Newtonian fluid is flowing. The diameter of the sphere D and the fluid viscosity μ, density ρ, and velocity V may vary. Each of the five variables can be expressed using various combinations of the three dimensions mass, length, and time (by Newton's second law, force equals mass times length per the square of time). The Pi theorem leads immediately to the conclusion that only two dimensionless numbers are needed to describe the relationship. These may be taken to be a drag coefficient $F_D/\frac{1}{2}\rho V^2\pi D^2/4$ and a Reynolds number $\rho VD/\mu$. An accurate set of measurements for one sphere in one fluid provides a universal relationship between these numbers that is applicable to all spheres in all Newtonian fluids, unless other phenomena, such as compressibility or the proximity of a free surface, are involved.

The strength of dimensional analysis lies in its ability to limit the number of studies that need to be made and to handle situations in which the governing equations are not known. It can even handle lack of geometrical symmetry by using ratios of important dimensions as additional dimensionless groups. Its weakness lies in the need to know which variables must be included and which can be ignored, and in its awkwardness when handling several variables that have the same dimensions, eg, densities in multiphase mixtures. This last difficulty reflects the fact that dimensional analysis is not capable of describing the functional relationship among the dimensionless groups, nor is it capable of describing how an empirical relationship might be extrapolated outside the range covered by the original data. It is not even capable of selecting the best set of dimensionless groups, because products, sums, quotients, and differences of dimensionless groups are also dimensionless. To achieve the simplest, most meaningful relationship and to judge how it might best be extrapolated, it is necessary for the investigator to use previous experience, similarity analysis, or physical insight.

Similarity analysis starts from the equation describing a system and proceeds by expressing all of the dimensional variables and boundary conditions in the equation in reduced or normalized form. Velocities, eg, are expressed in terms of some reference velocity in the system, eg, the average velocity. When the equation is rewritten in this manner certain dimensionless groupings of the reference variables appear as coefficients, and the dimensional variables are replaced by their normalized versions. If another physical system could be described by the same equation with the same numerical values of the coefficients, then the solutions to the two equations (normalized variables) would be identical and either system would be an accurate model of the other.

The principle can be illustrated by examining the Navier-Stokes equation 18 for incompressible flow with constant viscosity, in a gravitational field in which the body force per unit volume is $f_i = \rho g_i$, where g_i is the gravitational acceleration vector. All variables in the system can be expressed in dimensionless forms, indicated by asterisks. All lengths are made dimensionless by dividing them by a

fixed length L_o, which usually is a characteristic geometrical dimension of the problem. Velocity can be expressed as $U_i^* = U_i / V_o$ where V_o is a fixed reference velocity. Time is made dimensionless by the resulting time scale L_o / V_o, $g_i = g g_i^*$ and pressure is non-dimensionalized by a reference value P_o. Then, equation 18 can be written in dimensionless form as

$$\frac{\partial U_i^*}{\partial t^*} + \sum_{j=1}^{3} U_j^* \frac{\partial U_i^*}{\partial x_j^*} = \left[\frac{gL_o}{V_o^2}\right] g_i^* - \left[\frac{P_o}{\rho V_o^2}\right] \frac{\partial P^*}{\partial x_i^*} + \left[\frac{\mu}{\rho V_o L_o}\right] \sum_{n=1}^{3} \frac{\partial^2 U_i^*}{\partial x_n^{*2}}, \quad i = 1, 2, 3 \quad (26)$$

The dimensionless quantities in brackets are, respectively, identified as the reciprocal of the Froude number Fr, the Euler number Eu, and the reciprocal of the Reynolds number Re for the system. Considering that the Navier-Stokes equation is a momentum balance, one is reminded that the left hand side of equation 26 is the dimensionless acceleration of a fluid element, or, to adopt an old-fashioned expression, the opposite of a dimensionless "inertia force", while the three terms on the right-hand side are, respectively, the dimensionless gravitational, pressure and viscous forces. Two flow systems with geometrically similar boundaries in which all three dimensionless groups are matched would be governed by identical dimensionless equations and the solutions of one system would also apply to the other, provided that they are multiplied by appropriate scales. This is a mathematical proof of dynamic similarity.

In addition to the above important conclusion, similarity analysis also provides a means of simplifying the solution of a problem by order-of-magnitude analysis. Without claiming mathematical rigor, one may hypothesize that dimensionless properties are all of order one, reflecting the expectation that the scales have been chosen appropriately. Then, the orders of magnitude of the different terms in equation 26 can be estimated by the ratios of their coefficients. Thus, the Reynolds number may be viewed as representing the ratio of inertia force to viscous force. Of course, this Reynolds number is based on single values of the velocity and length scales and should describe the system only in a global sense, as the ratio of inertia and viscous forces may vary widely throughout the system. Even so, one may say that, when the Reynolds number is extremely small, viscous forces would dominate over inertia forces, and assert that fluid inertia (ie, acceleration) may be neglected in the analysis. Similarly, the Froude number represents the square root of the ratio of inertia force and gravitational force. When the Froude number is very large, gravitational effects may be neglected. In this procedure, one may compare the orders of magnitude of the different terms in equation 26 and neglect the ones that are much smaller than others.

In addition to the Reynolds, Froude, and Euler numbers, a large number of other dimensionless groups have been in use in fluid mechanics, heat transfer and related disciplines. A partial list is given below (16), while many others can be found in reference 10.

- Mach number:

$$\mathrm{M} = \frac{V}{c} \quad (27)$$

where c is the speed of sound; it represents the ratio of the inertia and elastic forces (compressibility).

- Prandtl number:

$$\mathrm{Pr} = \frac{\nu}{\gamma} = \frac{c_p \mu}{k} \tag{28}$$

where γ is the thermal diffusivity, c_p is the specific heat under constant pressure and k is the thermal conductivity of the fluid; it represents the ratio of the rates of diffusion of momentum and heat due to molecular motions.

- Schmidt number:

$$\mathrm{Sc} = \frac{\nu}{\gamma_c} \tag{29}$$

where γ_c is the molecular diffusivity of a species in a fluid mixture; it represents the ratio of the rates of diffusion of momentum and mass in the fluid.

- Weber number (for liquids):

$$\mathrm{We} = \frac{\rho V^2 L}{\sigma} \tag{30}$$

where σ is the surface tension; We represents the ratio of the inertia to the surface tension forces.

- Capillary number (for two-phase flows):

$$Ca = \frac{\mu V}{\sigma} \tag{31}$$

- Cavitation number (for liquids):

$$\sigma_c = \frac{P - P_v}{\frac{1}{2}\rho V^2} \tag{32}$$

where P_v is the vapor pressure.

- Nusselt number:

$$\mathrm{Nu} = \frac{hL}{k} \tag{33}$$

where h is the overall heat transfer coefficient and k is the thermal conductivity of the fluid; it represents the ratio of total and conductive heat transfer rates in a fluid.

- Grashof number:

$$\mathrm{Gr} = \frac{\alpha g L^3 \Delta T}{\nu^2} \tag{34}$$

where α is the thermal expansion coefficient and ΔT is a temperature difference; it represents the ratio of buoyancy force and viscous force.

- Péclet number:

$$\mathrm{Pe} = \frac{VL}{k} (= Re\,Pr) \tag{35}$$

it represents the ratio of heat convection and heat conduction.

- Rayleigh number (for free thermal convection):

$$\mathrm{Ra} = \frac{\alpha g L^3 \Delta T}{\upsilon k} = \frac{g \frac{\partial \rho}{\partial T} L^3 \Delta T}{\mu k} (= GrPr) \tag{36}$$

- Marangoni number (for convection induced by surface tension gradients):

$$\mathrm{Ma} = \frac{\frac{\partial \sigma}{\partial c} \frac{\partial c}{\partial x} L^2}{\mu \gamma_c} \quad \text{(for concentration gradients)} \tag{37}$$

$$\mathrm{Ma} = \frac{\frac{\partial \sigma}{\partial T} \frac{\partial T}{\partial x} L^2}{\mu \gamma} \quad \text{(for temperature gradients)} \tag{38}$$

- Richardson number (for density-stratified flows):

$$\mathrm{Ri} = -\frac{g\rho/h}{\rho(V/h)^2} = -\frac{gh}{V^2} = -\mathrm{Fr}^{-\frac{1}{2}} \tag{39}$$

  it represents the ratio of potential energy associated with gravity and kinetic energy.
- Taylor number (for rotating flows):

$$\mathrm{Ta} = \frac{\Omega^2 L^4}{\upsilon^2} \tag{40}$$

  where Ω is the rotation rate.
- Rossby number (for rotating flows):

$$\mathrm{Ro} = \frac{V}{\Omega L} \tag{41}$$

  it represents the ratio of inertia and Coriolis forces.
- Strouhal number (for periodic vortex shedding from bluff objects):

$$\mathrm{St} = \frac{fL}{V} \tag{42}$$

  where f is the frequency of vortex shedding.
- Knudsen number for gases:

$$\mathrm{Kn} = \frac{\lambda}{L} \tag{43}$$

where λ is the mean free path.

The principal difficulty faced by the experimenter in applying the results of dimensional or similarity analysis is that often there is insufficient freedom with respect to the physical properties of the modeling fluids to match all of the potentially important dimensionless groups. Construction and interpretation of the model rests largely on the experience and judgment of the experimenter as to which groups can safely be ignored within the accuracy desired. In some cases, useful results can be obtained even when none of the dimensionless groups can be matched. An example is the use of small-scale models in wind tunnels to study

the turbulent dispersion of materials released to the atmosphere in the vicinity of complex structures such as refineries or orchards. It may not be practical or possible to match the Reynolds number by increasing wind velocity in inverse proportion to the reduction in scale. Instead, use is made of the observation that, when the Reynolds number based on the characteristic dimension of the structure exceeds about 10^4, one can reasonably expect many average properties of the flows to be similar, ie, turbulent fluctuations to be proportional to the mean velocity and the wakes of the structures to be geometrically similar. Although flow fields around small elements of the structure are not duplicated, the overall error from this approximation is less than would result from an attempt to calculate the dispersion by combining the correlations for individual structures.

2.5. Turbulent Flows. Although the space-time dependence of velocity and pressure in turbulent flows is accurately described by the same general continuity and momentum equations as in laminar flows, turbulent properties change far too rapidly and randomly to be of interest in their entirety. In most engineering applications, interest lies instead in their statistical averages (17–19). The most general type of averaging is ensemble averaging, in which all properties are averages over a large number of repeated realizations of the same experiment (17–19). Then, one may introduce the Reynolds decomposition, by which an individual value of the velocity U_i at a time instant and location is decomposed into an average value $\langle U_i \rangle$, to be denoted by angle brackets, and a fluctuation u_i, to be denoted by a lower case symbol, ie,

$$U_i = \langle U_i \rangle + u_i \tag{44}$$

Similarly, the pressure is decomposed as

$$P = \langle P \rangle + p \tag{45}$$

By definition, the averages of fluctuations vanish, ie,

$$\langle u_i \rangle = 0, \quad \langle p \rangle = 0 \tag{46}$$

Under certain conditions, statistical properties may be considered as independent of time shift, in which case the flow is called stationary and time averages, to be denoted by overbars, can be defined as

$$\bar{U}_i = \lim_{T \to 0} \frac{1}{T} \int_0^T U_i dt \tag{47}$$

If the statistical properties of all independent realizations (ensemble members) coincide, in which case the flow is called ergodic, time averages would be the same as ensemble averages.

Equations governing statistical averages in turbulent flows can be obtained by substituting the Reynolds-decomposed properties into the equations of motion and then averaging all terms. Then, one would obtain the Reynolds-averaged equations. For example, applying this process to the continuity and momentum equations for an incompressible, Newtonian fluid with constant properties and in

the absence of body forces would lead to the set

$$\sum_{i=1}^{3} \frac{\partial \langle U_i \rangle}{\partial x_i} = 0 \tag{48}$$

$$\rho \frac{\partial \langle U_i \rangle}{\partial t} + \rho \sum_{j=1}^{3} \langle U_j \rangle \frac{\partial \langle U_i \rangle}{\partial x_i} = -\frac{\partial \langle P \rangle}{\partial x_i} + \mu \sum_{j=1}^{3} \frac{\partial^2 \langle U_i \rangle}{\partial x_j^2} - \rho \sum_{j=1}^{3} \frac{\partial \langle u_i u_j \rangle}{\partial x_j} \tag{49}$$

Unlike the original set of four equations that contained only four unknowns, $U_i, i = 1,2,3$, and P, the above set contains 10 unknowns, the four means $\langle U_i \rangle$, $i = 1,2,3$, and $\langle P \rangle$, and the nine turbulent or Reynolds "stresses" $\rho \langle u_i u_j \rangle$, only six of which are independent. The Reynolds stress $\rho \langle u_1 u_2 \rangle$, eg, is the rate at which x_1-momentum per unit volume ρu_1 is being transported in the x_2-direction by the velocity fluctuation u_2. Any attempt to produce additional equations for the Reynolds stresses, based on the basic equations of motion and statistical procedures, would introduce many more unknowns, such as averages of triple products of fluctuations. Thus, the Reynolds averaging process produces an open hierarchy of equations, which can only be closed by the introduction of turbulence models, namely empirical relationships among the various statistical properties. This topic will be further discussed in the section Computational Fluid Dynamics.

3. Specific Flows

3.1. Internal Flows. Flows that are confined by solid walls, except at inlet and outlet ports, are called internal. They include flows in pipes, ducts, channels and various types of machinery. On the boundary, the fluid exercises normal and shear stresses on the wall, which result on a force on the wall and pressure losses in the fluid. A common configuration is that of "fully developed" flow in a long, straight circular pipe with a uniform diameter, D, far from the entrance. In this case, the local mean flow velocity throughout the cross-section is parallel to the pipe axis and the pressure loss ΔP along a pipe section with length L can be expressed in dimensionless form by the friction factor:

$$f = \frac{1}{(L/D)} \frac{\Delta P}{\frac{1}{2} \rho U_b^2} \tag{50}$$

where U_b is the bulk velocity in the pipe, namely, the volumetric flow rate divided by the pipe cross-sectional area. The friction coefficient depends on the Reynolds number $\mathrm{Re} = \rho U_b D/\mu$ and the relative roughness e/D, where e is the wall roughness characteristic height.

Two distinct states of fully developed flow are observed in a pipe. At low Reynolds numbers, the flow is laminar and the fluid flows in concentric cylindrical sheaths or laminae that do not mix with each other. A stream of dye introduced into the fluid proceeds down the pipe as a thread, spreading only slightly by molecular diffusion. The velocity profile is parabolic, with the velocity

decreasing from twice the average velocity at the axis to zero at the wall. This is easily demonstrated by solving the Navier-Stokes equations, which take on a rather simple form in this configuration. The friction coefficient takes the simple theoretical form

$$f = \frac{64}{Re} \tag{51}$$

When the Reynolds number increases to nominally about Re $\approx$ 2, 100 for commercial pipes, an abrupt change occurs. Random instabilities, which decay at lower velocities, grow, destroying the laminar flow pattern. At Re $\approx$ 10,000, the transformation is nearly complete. This process is called transition to turbulence. The velocity over most of the pipe, called the core, becomes fairly uniform, about equal to the average velocity. Only in a thin region near the wall is the radial variation of the velocity substantial. Frictional losses for turbulent pipe flows cannot be predicted theoretically; instead, they are based on empirical correlations. For extremely smooth pipes, one may use the Blasius correlation

$$f = \frac{0.316}{Re^{1/4}} \tag{52}$$

while, for rough-wall pipes, a popular implicit relationship for f is the Colebrook correlation

$$\frac{1}{\sqrt{f}} = -2.0 \log\left(\frac{e/D}{3.7} + \frac{2.51}{Re\sqrt{f}}\right) \tag{53}$$

Most commonly, the friction factor is found from the Moody diagram, shown in Figure 3. Notice that, for a given e/D, the turbulent flow regime contains a high Reynolds number region in which f is essentially constant. This region is called the "fully rough" zone.

Pressure losses associated with fully developed pipe flow are termed as "major losses". All other losses, associated with the entrance region, flow area changes, direction changes, flow through valves and other devices and loss of kinetic energy at the exit, are collectively termed as "minor losses", even when they represent the majority of total losses. Additional losses occur in the entrance region of the pipe, where the flow velocity profile develops from a nominally uniform one towards its fully developed one. For laminar flow in a tube, the entrance length, defined as the distance required for the velocity at the center line to reach 99% of its asymptotic value, is given by

$$\frac{L_{ent}}{D} \approx 0.06Re \tag{54}$$

while, for turbulent flow, $L_{ent}/D \approx 25 \div 40$. Throughout the entrance region, the velocity gradient at the wall is larger than for the fully developed profile, producing a higher pressure drop and greater heat transfer per unit length than for fully developed flow. Although entrance phenomena are often ignored, these can be of significance, especially in capillary viscometers and compact (short

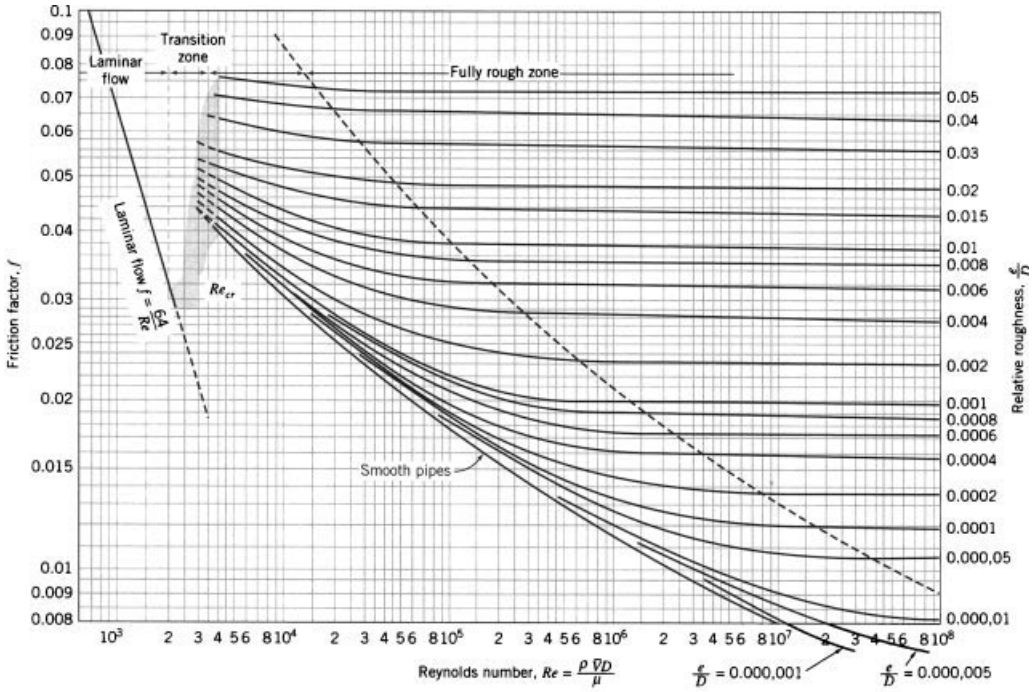

Fig. 3. Moody diagram showing the friction factor for fully developed pipe flow [reproduced from (1) with permission].

tube) heat exchangers. The entrance losses depend on the shape of the entrance and can be significantly reduced by using a bell-mouth entry. When a flow expands abruptly, separation occurs producing a jet of fluid flanked by recirculating eddies. For turbulent flows, separation occurs in a diverging duct when the angle of divergence exceeds $\sim 7^\circ$. When separation occurs, the ability of the fluid to recover pressure upon deceleration is seriously impaired because the kinetic energy is lost to friction. When the ratio of duct areas is large, all of the kinetic energy is lost and no pressure is recovered. Further details about minor losses in pipes can be found in standard references (1-3,6,13).

Although the above discussion concerns circular pipes, it can be approximately applied to ducts and open channels with different cross-sectional shapes, if the pipe diameter D is replaced by the hydraulic diameter

$$D_h = \frac{4A}{P} \tag{55}$$

where A is the cross-sectional area filled with flowing fluid and P is the wetted perimeter, namely, the part of the perimeter that is in contact with the fluid. The appropriate Reynolds number would be based on D_h and the actual bulk velocity U_b.

3.2. Flows Near Solid Walls. Except at very low Reynolds numbers, the flow field past immersed solid boundaries can be divided into two reasonably well-defined regions: a thin region close to the surface, called the boundary layer, in which the gradient of tangential velocity is large and shear stresses are

important; and a region away form the boundary, called the free stream, in which velocity gradients are small, resulting in small or negligible viscous stresses. The concept of the boundary layer was originally developed by Prandtl (20). The edge of the boundary layer is taken to be the point at which the velocity differs from that in the free stream by some small amount, say 1%. This approximation allows the main flow field and the normal stresses on the surface to be calculated by solving Euler equations, or even easier, Laplace's equation for the velocity potential, with the boundary layer calculation then appended to yield the shear stresses at the surface. Extensive treatises have been devoted to analyzing flows in terms of boundary layer phenomena (12,21,22). Although boundary layer analysis is widely applicable, it can fail badly in regions of strong deceleration where the boundary layer flow can separate under the influence of the unfavorable pressure gradient imposed by the main flow. This is illustrated in Figure 4, showing separation of a laminar boundary layer from the surface of a circular cylinder, at Re $\approx$ 1,000. Separation is a result of the inability of the slowly moving fluid near the surface to move against an increasing pressure gradient. As the bulk of the fluid passes over the forward face of the cylinder and accelerates, it decreases in pressure. The fluid in the boundary layer also accelerates, although by a much smaller amount because of the retarding effects of viscous stresses. Over the rear face of the cylinder, the bulk fluid decelerates and pressure rises. This pressure gradient decelerates the already slowly moving fluid near the boundary, brings it to rest, and, as pressure continues to rise, reverses the flow at the surface and lifts the boundary layer. The position at which the wall shear stress becomes zero is the point of separation.

When the flow is bounded on only one side, the boundary layer can, in theory, grow indefinitely, albeit slowly, into the surrounding fluid. Flow past a smooth flat plate illustrates this behavior. As the fluid passes the leading edge of the plate, a boundary layer begins to grow. Initially this layer is laminar and its profile and growth rate can be calculated easily by solving the Navier-Stokes equations using the concept of boundary layer approximation; this is known as the Blasius solution and applies to all two-dimensional, laminar boundary layers over plane walls (1). The boundary layer grows steadily with

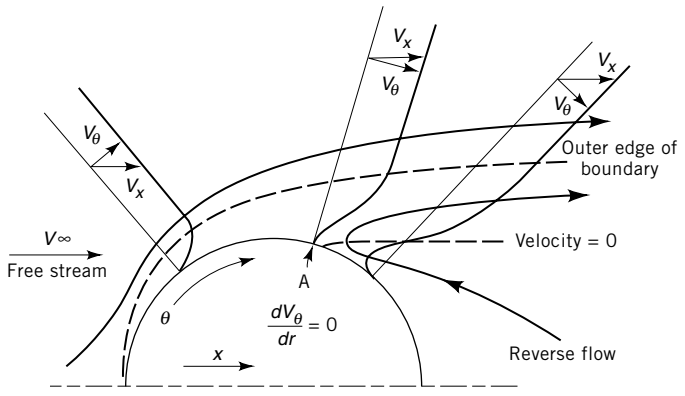

Fig. 4. Boundary layer development and separation from the surface of a smooth circular cylinder at $Re^{1/4}$ 1000; A is the separation point.

distance x from the plate's start. When the Reynolds number $\rho x V_\infty/\mu$ (V_∞ is the uniform free stream velocity) reaches a typical value of $\sim 4 \times 10^5$ for practical configurations, the laminar boundary has grown so thick that it is unstable to even small disturbances. The oscillations caused by disturbances from the outer flow are not damped but are transformed into vortices that break down into the random eddies of turbulence. This process, called transition to turbulence, is almost complete when the Reynolds number reaches $\sim 4 \times 10^6$. Turbulence allows a higher rate of transfer of momentum within the fluid; consequently, transition is accompanied by a considerable increase in the thickness of the boundary layer. The turbulent boundary layer can be further subdivided into: a viscous (or laminar) sublayer, which is a very thin layer in contact with the wall and in which viscous stresses dominate over turbulent stresses and the flow velocity grows linearly with distance form the wall; a buffer sublayer, intermediate between the viscous and the logarithmic sublayer; a logarithmic sublayer, in which the mean velocity follows a logarithmic variation with respect to distance from the wall; up to the edge of the logarithmic sublayer, one may reasonably assume that flow properties are universal and apply to all turbulent boundary layers; and an outer sublayer, whose properties depend strongly on the geometry and Reynolds number.

3.3. Flows Past Solid Bodies. A fluid moving past a solid body exerts a drag force on the solid. Both shear stresses and normal stresses can contribute to the drag, commonly referred to as skin friction drag and form or pressure drag, respectively. Their relative importance depends on the shape of the body and the Reynolds number. Body shapes (eg, wings) for which skin friction drag predominates are called streamlined, while those shapes (eg, buildings) for which form drag dominates are called bluff. At extremely low Reynolds numbers (eg, <1), skin friction drag always dominates. The combined drag force is expressed in terms of the dimensionless drag coefficient:

$$C_D = \frac{F_D}{\frac{1}{2}\rho A V^2} \tag{56}$$

where A is the frontal area, namely the projected area normal to the stream. At very low Reynolds numbers (Re <1), C_D for all bluff objects varies inversely proportionally to the Reynolds number (for spheres, the Stokes solution is $C_D = 24/\mathrm{Re}$), while at high Reynolds numbers (typically Re >1000), C_D is nearly constant, with the exception of the critical Rerange, observed for objects with rounded contours, but not those with sharp edges. The variations of C_D with Reynolds number for flows past smooth spheres and circular cylinders are shown in Figure 5.

The variation of drag coefficient is closely associated with the flow pattern around the object, which depends both on the body shape and the Reynolds number. As an example, Figure 6 shows such flow patterns for a high length-to-diameter ratio, smooth circular cylinder with its axis perpendicular to the stream and the different ranges are summarized below.

- $Re \ll 1$ (roughly up to 1): The flow around the cylinder is nearly symmetrical front-to-back as well as side-to-side. Fluid passing near the cylinder

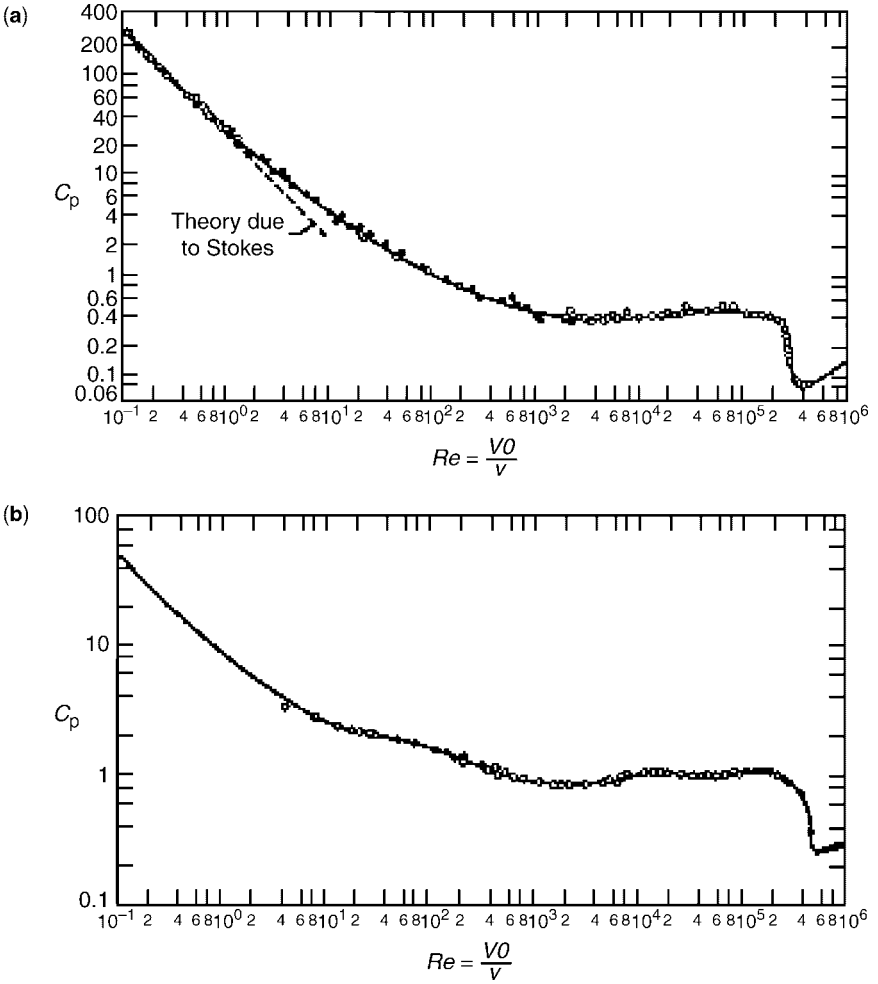

Fig. 5. Drag coefficient for smooth spheres (**a**) and circular cylinders (**b**); from (1), with permission.

accelerates over the upstream face and decelerates over the downstream face. Normal stresses on these faces largely cancel each other and drag results almost entirely from skin friction.

- $1 < Re < 4$: As Re increases, the flow becomes increasingly asymmetrical. Under the influence of fluid inertia, the fluid streamlines crowd together on the upstream face of the cylinder and spread further apart on the downstream side. This imbalance is reflected in an imbalance in normal stresses and the emergence of form drag.
- $4 < Re < 47$: Flow separation occurs symmetrically on the downstream side; the fluid flowing next to the surface of the cylinder departs abruptly from the surface, the gap formed being filled by a pair of recirculating, laminar

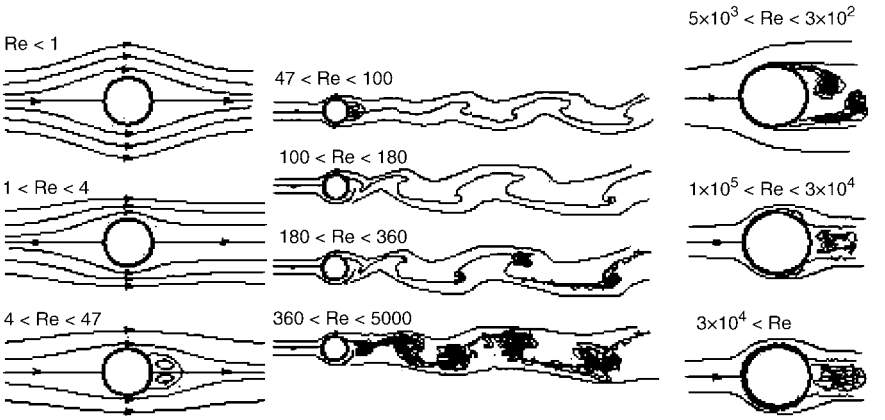

Fig. 6. Sketches of vortex patterns behind a circular cylinder with its axis perpendicular to a stream.

vortices that remain attached to the cylinder's aft; the wake is laminar and steady, but starts oscillating far downstream for Re >40.

- 47< *Re* <100: Although the vortex pair remains attached, the wake becomes unstable rapidly and forms a series of alternating laminar vortices (Karman vortex street).
- 100< *Re* <180: The vortices behind the cylinder are no longer attached, but released alternately into the wake, forming a vortex street from the start, but which remains laminar far downstream of the cylinder.
- 180 < *Re* <360: At some downstream distance, the vortex street undergoes a laminar-to-turbulent transition.
- 360< *Re* <5000: The shear layer between the free stream and the retarded fluid becomes unstable from the start and soon afterwards turbulent; in this range, the drag coefficient becomes nearly independent of Reynolds number and the pressure on the downstream side of the cylinder is almost constant, roughly equal to the low value at the point of separation; this results in a considerable imbalance of pressure between the upstream and downstream surfaces and make form drag dominant over skin friction.
- $5 \times 10^3 < Re < 2 \times 10^5$: This is called the subcritical regime; in this regime, laminar boundary layers form on the two sides of the cylinder and separate alternately at about $\theta \approx 80–85^\circ$; the shed vortices are turbulent from the start and the wake is quite wide; the drag coefficient is near 1 and insensitive to Re.
- $2 \times 10^5 < Re < 3 \times 10^6$: This is the critical regime, in which the boundary layer separates as in the subcritical regime, but then becomes turbulent; the higher mixing due to turbulence brings faster fluid near the wall, which can resist adverse pressure forces better and reattaches to the wall; the turbulent boundary layer remains attached until $\sim\theta \approx 110–120^\circ$, where it separates and forms vortices; in this range, the wake is much narrower than in the previous one and the form drag decreases dramatically, as the

wall pressure in the range $90^\circ \ \theta \ 120^\circ$ recovers to higher values; as a result, the drag coefficient undergoes a sudden downward step change; the wake is quite disorganized and the vortex street is not evident; the laminar-to-turbulent transition in the boundary layer, and associated drag reduction, can be triggered at lower Reynolds numbers by roughening the surface with sand grains or a trip wire.

- 3×10^6 Re: This is the supercritical regime, in which the boundary layer is fully turbulent along the cylinder's surface and separates at $\sim\theta \approx 110$–120°, as in the previous regime; although the wake is still narrow, additional skin friction due to turbulence increases the drag coefficient to near its subcritical value of ~ 1; the vortex street is once more well defined.

The periodic vortex shedding produces lateral forces of the same period on the cylinder. Should the cylinder be weakly supported and have a natural frequency close to the shedding frequency, it would oscillate strongly in concert with the vortex street, a phenomenon known as vortex induced vibration. Flow induced vibration is much more likely to happen for elongated (eg, cylinders) rather than compact (eg, spheres) bodies. Such behavior is responsible for the singing of power lines, failure of shell-and-tube heat exchangers, the oscillation of tall smokestacks, and, most spectacularly, for the collapse in 1940 of the newly built Tacoma Narrows suspension bridge, in Washington state, under the influence of a steady 65-km/h wind. The vortex shedding frequency f is usually presented in dimensionless form, as the Strouhal number

$$\mathrm{St} = \frac{fD}{V} \tag{57}$$

where D is a frontal dimension of the object. The Strouhal number depends on the shape of the object and the Reynolds number, tending to a near constant value at large Reynolds numbers for object shapes with sharp edges, which do not have a critical regime. For bodies with a critical regime, St fluctuates dramatically when the Reynolds number is within this regime. The variation of Strouhal number for circular cylinders is shown if Figure 7. It can be seen that over a wide range of Reynolds numbers, $\mathrm{St} \approx 0.20 \pm 0.1$.

Besides the drag force, the character of the flow also affects the heat and mass transfer to the surface. At low Reynolds numbers, the thinner boundary layer on the upstream face of the cylinder exhibits a higher heat-transfer coefficient than does the thickened layer on the downstream face. Despite the onset of separated flow and the large energy losses in the wake, the upstream coefficient remains larger until the Reynolds number reaches $\sim 5 \times 10^4$. Above this point the washing of the surface by the shedding eddies makes the downstream coefficient larger. The point of maximum heat transfer occurs at the forward stagnation point ($\theta = 0^\circ$, in Fig. 4) for Re $< 5 \times 10^4$, at the rear stagnation point ($\theta = 180^\circ$) for $5 \times 10^4 <$ Re $< 2 \times 10^5$, and at an intermediate location ($\theta \approx 115^\circ$) for Re $> 2 \times 10^5$. Minimum heat transfer occurs near the point of separation.

When the contour of the immersed object is rounded, as in the case of circular cylinders, spheres and the like, separation points are free to move along the surface, depending on the Reynolds number, the surface roughness and the flow

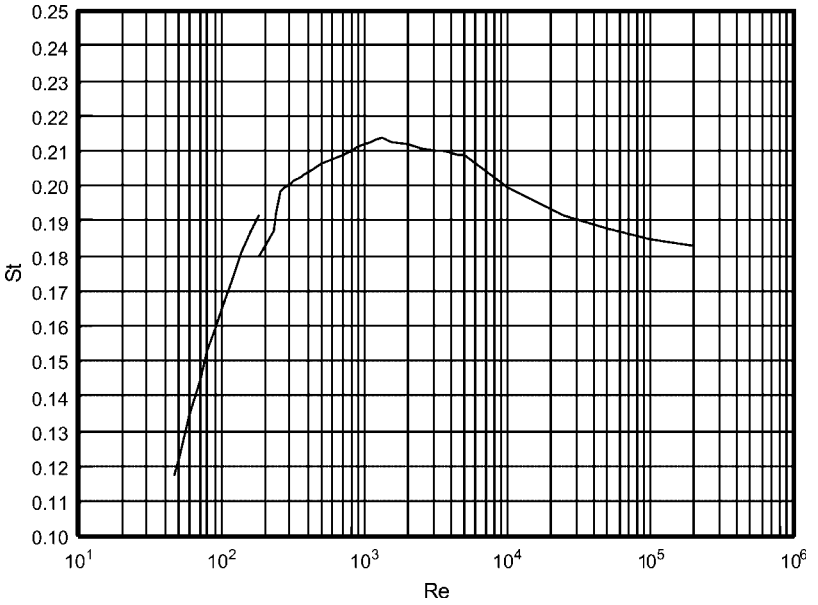

Fig. 7. Variation of Strouhal number with Reynolds number for a circular cylinder with its axis perpendicular to a stream [adapted from (23)].

disturbances. When, however, the object has sharp corners or edges, as in the case of a rectangular cylinder, separation always occurs at these edges and no critical regime is observed. In most technological processes, flow separation is undesirable and effort is made to eliminate or reduce it by redesigning the object shape (eg, streamlining), applying suction or tangential fluid injection, or using various control devices. Drag coefficients and Strouhal numbers for a variety of body shapes can be found in reference (6).

3.4. Free Shear Flows. These are flows which are confined not by solid boundaries, but by fluid at a different speed. Simple shear flows include jets, in which a stream is injected into slower surroundings, wakes, in which the stream has been retarded by the presence of an upstream object, mixing layers, which are the regions between two parallel streams of different speeds, and plumes, which are fluid columns rising due to buoyancy. Jets are used industrially to perform many mixing operations ranging from gradual mixing of tanks to the rapid mixing needed in chemical reactors or flames. Mixing in turbulent wakes is important in the disposal of wastes at sea and in the dispersion of potential atmospheric pollutants downwind of structures. Much interest in plumes is centered around the behavior of gases emitted from smokestacks into the atmosphere. The flow field in a jet, wake or plume may be regarded as a shear layer that grows by entraining fluid from its surroundings. Free shear flows may be either laminar or turbulent, although most important applications involve turbulent ones, which begin to form when the Reynolds number, based on a velocity difference and a characteristic transverse width, exceeds a critical value, typically a few hundred. Near their physical origin, turbulent free shear flows have an entry region (see example in Fig. 8), in which the flow patterns develop and are strongly affected

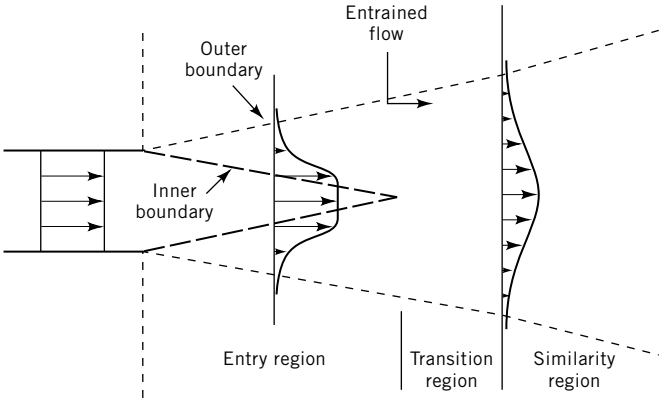

Fig. 8. Sketch of a jet, showing the entry, transition and similarity regions.

by the starting conditions. Several initial widths downstream from the origin, a fully developed region forms, where the velocity profiles, made dimensionless by the maximum velocity difference $\Delta U_{\max}$ and plotted vs. the transverse distance normalized by the local characteristic width w, are universal and independent of the starting conditions (self-similar profiles). Simplified analysis, mostly confirmed experimentally, predicts that these two characteristic scales evolve with downstream distance x from the origin following power laws, as

$$\Delta U_{\max} \propto x^{-m} \tag{58}$$

$$w \propto x^{n} \tag{59}$$

The exponents in these laws have been summarized in the table below (19,24).

Flow type	m	n
two-dimensional wakes	1/2	1/2
axisymmetric wakes	2/3	1/3
two-dimensional jets in still fluid	1/2	1
axisymmetric jets in still fluid	1	1
two-dimensional mixing layers	0	1
two-dimensional plumes	0	1
axisymmetric plumes	1/3	1

Mass and heat transport within the shear flow follow the same general pattern as does momentum transport. For gases, it is found experimentally that the thermal or concentration jet spreads somewhat faster and decays more rapidly than does the momentum jet. All can be described by the turbulent equations of motion and useful results can be obtained by using eddy diffusivities, which are nearly constant across the jet but decrease with downstream distance. The concentration jet, because of its association with a particular chemical

species, remains identifiable longest, even though the jet velocity may be indistinguishable from that of the surrounding fluid. An important example involving concentration of pollutants is the plume released from a smokestack or vent. Except right at the source, the behavior of the plume is dominated by its buoyancy and/or the turbulence of the fluid into which it is injected. Figure 9 describes several of the plume patterns that can be obtained as they are affected by the vertical temperature variation in the surrounding air (25). The quantitative description of the dispersion of such plumes, especially their ground-level concentration, is still imperfectly developed and one must usually resort to empirical correlations. Where the effects of buoyancy are subordinate to the effects of wind velocity, useful results for dispersion over complex terrain or around structures can be obtained by wind tunnel experiments using scale models.

Most of the remarks above refer to unconfined or free flows. Many industrial applications involve the use of confined jets. It is customary to consider a jet confined when the ratio of the confinement radius to the source radius lies in the range 4–100. Below a ratio of 2, the jet does not develop its similarity profile before striking the wall, whereas above a ratio of 100 the jet itself may usually be considered free. Under certain conditions, flow in confined jets is accompanied by the existence of a recirculation zone, which significantly affects

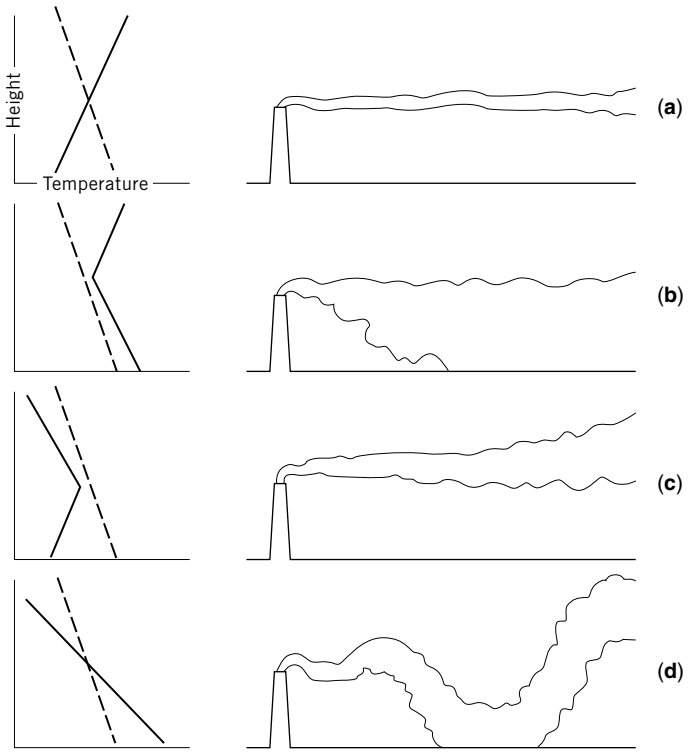

Fig. 9. Characteristic plume patterns: (**a**) fanning; (**b**) fumigation; (**c**) lofting; and (**d**) looping; dashed lines represent the adiabatic temperature and solid lines the actual air temperature. Courtesy of Scientific American (27).

the jet behavior by returning material upstream (26). This recirculation can be particularly important in combustion processes.

3.5. Compressible Flows. The flow of easily compressible fluids, ie, gases, exhibits features not evident in the flow of substantially incompressible fluid, ie, liquids. These differences arise because of the ease with which gas velocities can be brought to or beyond the speed of sound and the substantial reversible exchange possible between kinetic energy and internal energy. The Mach number, the ratio of the gas velocity to the local speed of sound, plays a central role in describing such flows.

Consider the converging-diverging nozzle described in Figure 10, and for simplicity consider only isentropic (ie, frictionless and adiabatic), one-dimensional flow. When the pressures in the upstream and downstream reservoirs are equal, no flow occurs, A. When the pressure in the downstream reservoir is reduced, flow commences. In the converging section, velocity increases with distance, and both pressure and temperature fall in accordance with the overall energy balance and the equation of state. In the diverging section, the fluid slows and some pressure is recovered, B. As the downstream pressure is reduced further, the behavior remains qualitatively the same until a point is reached at which the velocity in the nozzle throat equals the local speed of sound. At this point it is found that there are two possible paths that the downstream flow can follow and remain thermodynamically reversible. One corresponds to recompression and deceleration to subsonic flow C, the other to further expansion and acceleration to supersonic flow G. Operation at an intermediate pressure in the

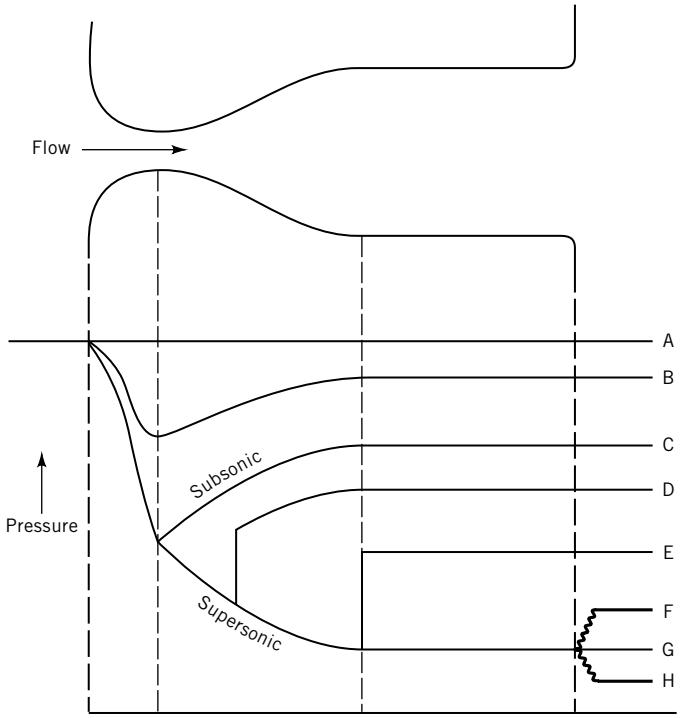

Fig. 10. Pressure variation in compressible flow through a converging-diverging nozzle.

reservoir D is possible only by sacrificing thermodynamic reversibility. Under these circumstances, a standing normal shock front is set up at some point in the diverging section. At this front, pressure, temperature, and entropy rise, and velocity drops abruptly over a distance of a few molecular mean-free paths. Flow changes from supersonic upstream of the shock to subsonic downstream. The relationship between the two conditions is established by conservation of energy and by conservation of momentum across the shock front.

Further reductions in reservoir pressure move the shock front downstream until it reaches the outlet of the nozzle E. If the reservoir pressure is reduced further, the shock front is displaced to the end of the tube, and is replaced by an oblique shock, F, continuous flow without pressure change, G, or an expansion fan, H, at the tube exit. Flow is now thermodynamically reversible all the way to the tube exit and is supersonic in the tube. In practice, frictional losses limit the length of the tube in which supersonic flow can be obtained to no more than 100 pipe diameters.

While the behavior downstream of the throat is displaying these complexities, nothing is changing upstream. Once the velocity at the throat becomes sonic, no downstream perturbation, eg, a sound wave, can be propagated upstream. Throughout the change from C to H the mass rate of flow remains constant at the value first established at C. An increase in flow can be accomplished only by raising the upstream pressure. In the absence of any temperature change in the upstream reservoir, the increase in flow results solely from a change in fluid density, not from a higher velocity in the throat. This isolation of flow rate from downstream effects can be employed to meter gases through orifices or nozzles at a constant rate, irrespective of downstream fluctuations. For ideal gases and relatively low upstream velocities, sonic flow through the throat is established whenever the ratio of upstream to downstream pressure across the constriction exceeds the quantity

$$\left(\frac{\gamma+1}{2}\right)^{\frac{\gamma}{\gamma-1}} \tag{60}$$

where γ is the ratio of specific heats for the gas; for air, $\gamma = 1.41$.

Phenomena analogous to shock waves in gases can occur in open-channel flow of liquids. The Froude number also represents the ratio of fluid velocity to the velocity of a small surface wave, and plays the same role in open-channel flow as the Mach number does in compressible flow. Thus, liquid flowing under a sluice gate is often discharged at a shallow depth at high velocity, corresponding to a Froude number greater than unity. At a distance downstream, the liquid is observed to undergo a hydraulic jump to a greater depth at a slower velocity, for which the Froude number is less than unity. The decreased liquid momentum appears as greater pressure (depth). In contrast to the normal shock, a great deal of turbulence is generated at the jump because of the sudden lateral expansion, and energy is dissipated through friction.

3.6. Flow Instability and Secondary Flows. In many flow situations it is found that a mathematically valid solution to the Navier-Stokes equations is closely verified by experiment over some ranges of the variables, but when the

variables are changed new flow patterns that are not in keeping with that solution are observed. The change is often rather sudden, and may involve a change from an unstable laminar solution to another, stable, laminar one or may involve transition to turbulence. Such behavior occurs because solutions to the Navier-Stokes equations are generally not unique. When more than one solution exists, it is possible to observe one flow pattern under one set of circumstances and a different pattern under another. At the present stage of development of fluid mechanics, an experiment must be performed to determine whether a given solution applies. In some cases, however, it is possible to determine the criteria by which one flow pattern becomes unstable in favor of another by analyzing the equations of motion. This analysis is the topic of a field called hydrodynamic stability. The simplest mathematical technique used in stability analysis starts from a known solution to the equations and then uses linearized versions of related equations to determine whether a small perturbation superimposed on this solution grows or decays as time passes. More advanced, nonlinear, stability analysis methods have also been developed, capable to determine not only the onset of instability, but also characteristics of the new flow patterns (eg, the wavelength of a periodic solution).

Fluids in Motion. Many of the instabilities associated with fluids in motion are of the shear-flow type, in which the velocity varies principally in a direction perpendicular to the flow direction. Examples include pipe flow, boundary layer flow, jet flow, and wake flow. At low Reynolds number, such flows have laminar solutions, which can be found by solving the Navier Stokes equations. As the Reynolds number increases above a certain value, which is different for each flow configuration, these solutions no longer describe the flow, which becomes unstable and changes possibly to another laminar state but eventually from laminar to turbulent. In boundary layer flows over smooth plane walls with extremely low external disturbances, the instability, usually referred to as Tollmien-Schlichting instability, occurs in essentially four steps (28): first, small two-dimensional waves form and are linearly amplified; second, the two-dimensional waves develop into finite three-dimensional waves and are amplified by nonlinear interactions; third, a turbulent spot forms at some localized point in the flow; and, finally, the turbulent spot propagates until the spot fills the entire flow field with turbulence. While at low Reynolds numbers viscosity damps out the instability, at high Reynolds numbers viscosity provides the destabilizing mechanism. Stability analysis cannot predict transition for pipe flow, as it predicts that laminar flow in pipes is stable at all values of the Reynolds number. Experimentally, the laminar-turbulent transition is found to occur at a Reynolds number of $\sim$2100, although by careful design of the experiment it can be delayed to Re as high as 40,000, or even higher.

In free shear flows, such as jets and wakes, there occurs another type of instability, called Kelvin-Helmholtz instability. This instability may be illustrated by considering the development of a small disturbance in the flow situation given in Figure 11. Suppose that a small disturbance causes a slight waviness of the boundary between the two flows. The fluid on the convex sides of each flow moves slightly faster and that on the concave sides moves slightly slower. According to the Bernoulli equation, this disturbance decreases the pressure on the convex sides of each flow, and thus the initial disturbance is

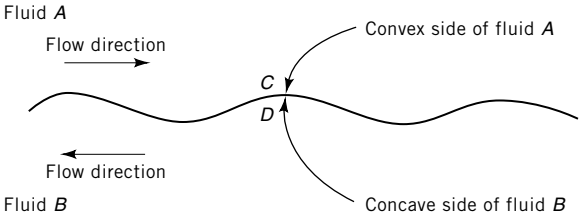

Fig. 11. Sketch of Kelvin-Helmholtz instability, where C, the convex side of fluid A, is at a lower pressure than D, the concave side of fluid B.

amplified. Kelvin-Helmholtz instability is also observed in horizontal concurrent flows of stratified immiscible fluids (Fig. 12). Raising of a wave at the interface forces the upper fluid to increase in velocity and drop in pressure as it passes the wave. If the pressure decrease is large enough, it overcomes the increase in potential associated with the raising of the wave and the disturbance grows.

An instability involving transition from one laminar flow pattern to another, called Taylor instability, occurs in the flow between coaxial cylinders in relative rotation with respect to each other. When the inner cylinder is rotated at an angular velocity below a critical value, motion is purely circumferential, called circular Couette flow. Above this value, however, centrifugal force destabilizes the flow and a series of laminar, cellular vortices known as Taylor cells are superimposed on the main flow (Fig. 13). The pattern of cells depends on the geometry and whether the outer cylinder is stationary or also rotating. As the angular velocity is increased, the cells become wavy and then irregular. At still higher velocities the cells break up and the flow becomes turbulent. If only the outer cylinder is rotated, Taylor cells do not form, and this arrangement is customarily used in Couette-type viscometers so as to maximize their useful ranges of shear rates.

When a fluid of low viscosity is used to displace a fluid of higher viscosity from a porous medium or a pipe, the displacement can become unstable by a process known as fingering. Small fingers of the low viscosity fluid, once formed, become regions of lower pressure drop. The displacing fluid flows preferentially

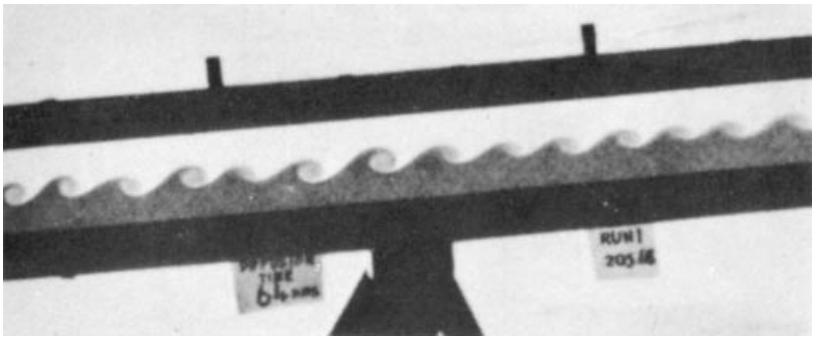

Fig. 12. Shear instability in stably stratified fluid; lower denser fluid is dyed. Courtesy of Cambridge University Press (29).

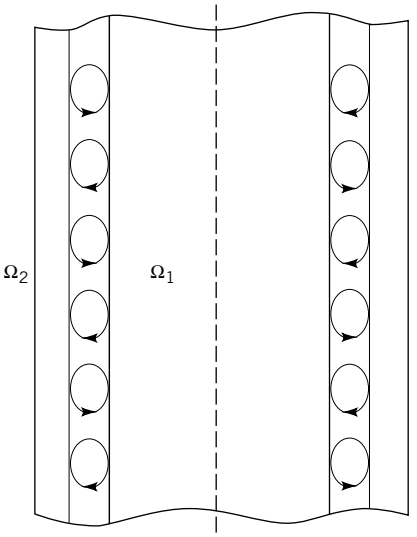

Fig. 13. Flow pattern in rotating Couette flow where Ω_1 and Ω_2 represent the outer and inner rotational speeds. Courtesy of Cambridge University Press (30).

into these fingers which grow and ultimately reach the outlet, leaving a portion of the viscous fluid undisplaced. Such displacements are widely practiced to increase the productivities of oil fields, and much effort is devoted to minimizing fingering by proper adjustment of the physical and chemical properties of the displacing medium, as well as of the rate of displacement.

Fluids at Rest. Fluids at rest may be set into motion by impressing upon them gradients in body or surface forces. Benard instability refers to the formation of convection cells within a fluid as a result of the action of a gravitational field on density differences induced by a temperature gradient in the fluid. Such behavior is observed, eg, when fluid is confined between two horizontal plates of which the lower one is heated. The heated fluid on the bottom expands, resulting in an unstable density gradient and providing a driving force to redistribute the fluid. Redistribution is inhibited by viscosity, which slows the flow, and by thermal conductivity, which tends to even out the temperature differences. The onset of instability is described by a critical Rayleigh number Ra (see the section Dimensional Analysis, Similarity and Modeling), based on the distance between the two plates. Hot fluid rises on one side and cold fluid falls on the other side of the cell. The rising fluid cools down as it nears the top, and the falling fluid warms up as it nears the bottom, thus maintaining a steady circulation.

Cellular motions may also arise from gradients in surface tension caused by variations in temperature or concentration. This behavior is commonly referred to as Marangoni instability. To illustrate this, consider a solution from which a volatile solute is evaporating and suppose the surface tension of the solution decreases as the concentration of solute increases. Because the solute is evaporating, the surface has a lower concentration of solute than the bulk. If a small disturbance occurs and causes a spot of high solute concentration (low surface

tension) to appear, this spot spreads. Spreading is a result of the attempt by the interface to minimize its free energy by expansion of regions of low surface tension and contraction of those of high surface tension. The local spreading is accompanied by movement of fluid from the bulk to fill the spreading spot. Because the new fluid has lower surface tension too, the original disturbance is amplified and convection cells are established. In some cases, the driving force is so strong that the surface undergoes violent twitching with a large increase in the overall mass-transfer rate. Such motion is commonly termed interfacial turbulence. If the direction of mass transfer is reversed, disturbances usually are not amplified and the surface remains quiescent. This effect is responsible for the occasionally observed large differences in mass-transfer rates for absorption and desorption in otherwise the same system. The transfer of acetic acid between water and carbon tetrachloride is a classic example. Circulation of fluid is promoted by surface tension gradients but inhibited by viscosity, which slows the flow, and by molecular diffusion, which tends to even out the concentration differences. The onset of instability is described by a critical Marangoni number Ma (see the section Dimensional Analysis, Similarity and Modeling), which is analogous to the Rayleigh number. Linear stability analysis has been successfully applied to derive the critical Marangoni number for several situations.

Surface tension is also responsible for the varicose or Rayleigh breakup of liquid strands into droplets. By virtue of surface tension the pressure within a non-planar strand would be different from that in the ambient gas by the amount:

$$\Delta P = \sigma\left(\frac{1}{R_1} + \frac{1}{R_2}\right) \tag{61}$$

where R_1 and R_2 are the principal radii of curvature of the interface. A small reduction in the radius results in a locally higher pressure than in the rest of the strand, causing liquid to flow away from that region, reducing the radius still further and making the thread unstable. Rayleigh analyzed this phenomenon for a low velocity, inviscid, cylindrical jet. He determined that one wavelength of disturbance grows more rapidly than all others and thus, in the absence of forced oscillations, determines the drop diameter. For an inviscid fluid this is about twice the strand diameter. At higher flows, a jet undergoes sinuous breakup in which the entire strand oscillates like a vibrating string. At still higher rates, as in commercial swirl atomizing nozzles, the liquid exits as a sheet that undergoes Kelvin-Helmholtz breakup into thread-like rings, which in turn disintegrate further, via Rayleigh instability, into fine droplets. The drop size produced is a function primarily of nozzle diameter D, fluid velocity V, and liquid properties ρ_l,μ_l. One widely used empirical correlation (31) yields the average (Sauter) droplet diameter as

$$d_{p,av} \propto D^{0.65} V^{-0.55} \rho_l^{-0.35} \rho^{0.2} \mu_l^{0.15} \tag{62}$$

Secondary Flows. In many cases, a cursory examination of the flow pattern might indicate a rather simple type of flow with a high degree of symmetry,

whereas in fact the flow realized is more complex. In the flow around a bend, eg, one might imagine that the individual streamlines simply follow the general course of the curvature of the pipe; in fact they do not. Instead, a pattern of secondary flow develops that is superimposed on the main flow so that the streamlines are actually helical. The choice is somewhat arbitrary as to which flow to call main and which to call secondary. Adopting the convention that the main flow is parallel to the tube axis, then at the axis the secondary flow is directed outward toward the section of pipe having the weakest curvature, returning inward along the pipe wall. This type of secondary flow is a consequence of the inertia of the fluid. It is most obvious at low Reynolds numbers, but is also significant in turbulent flow. By improving the lateral transport of momentum it postpones the transition from laminar to turbulent flow. Even relatively small curvatures can have a significant effect as is evidenced by the empirical correlation for helical tubes (D is the tube diameter and D_{hel} is the diameter of the helix):

$$Re_{transition} \approx 2100\left(1 + 12\sqrt{\frac{D}{D_{hel}}}\right) \tag{63}$$

Secondary flows also occur in channels that have polygonal cross-sectional shapes, but are otherwise straight. In these cases the secondary flows are directed outward into the corners and return along the walls. Such secondary flows are associated with gradients in turbulent stresses and only occur in turbulent flows. Many other types of secondary flows have been observed, when the main mechanism generating an axial flow finds competition in a secondary mechanism, which tends to generate transverse components.

3.7. Flow in Porous Media. Flow of fluids through fixed beds of solids occurs in situations as diverse as oil-field reservoirs, catalyst beds and filters, and absorption towers (2). The complex interconnected pore structure of such systems makes it necessary to use simplified models to make practical quantitative predictions. An important parameter is the porosity or void fraction ε, defined as the average fraction of the cross-section that is not occupied by the solid. One of the more successful treatments of single-phase pressure drop through such systems employs the results for flow through tubes, using average velocities and tube diameters. The average velocity through the pores V_l is called the interstitial velocity V_l, while the apparent velocity based on the entire cross-section V_S is called the superficial velocity. The two are related as

$$V_l = \frac{V_S}{\varepsilon} \tag{64}$$

A hydraulic diameter D_h for a porous medium can be defined as twice the ratio of the volume open to the flow and the wetted surface. For porous media with spherical particles of diameter d_p,

$$D_h = \frac{\varepsilon}{1-\varepsilon}\frac{d_p}{6} \tag{65}$$

Then, one may define a Reynolds number for flow through a porous medium as

$$Re_{por} = \frac{\rho V_S d_p}{\mu(1-\varepsilon)} \tag{66}$$

Pressure losses in flow through a porous medium are represented in dimensionless form by the friction factor

$$f_{por} = \frac{\varepsilon^3}{1-\varepsilon}\frac{1}{\rho V_S^2}\left(-\frac{\partial P}{\partial x}\right) \tag{67}$$

Empirical results for pressure losses through pipes randomly packed by spherical particles throughout the Reynolds number range are described by the Ergun relationship

$$f_{por} \approx 1.75 + \frac{150}{Re_{por}} \tag{68}$$

obtained by interpolation between the low- Re_{por}, laminar flow, Blake-Kozeny relationship

$$f_{por} \approx \frac{150}{Re_{por}}, \quad Re_{por} < 10 \tag{69}$$

and the high- Re_{por}, turbulent flow, Burke-Plummer relationship

$$f_{por} \approx 1.75, \quad Re_{por} > 1000 \tag{70}$$

For nonspherical particles, equivalent spherical diameters are employed and additional corrections for shape are introduced. When considering flow of water or oil through soil and rocks, it is customary to introduce an empirical permeability κ and compute pressure losses by Darcy's law (z is the vertical elevation)

$$-\frac{\partial P}{\partial x} - \rho g \frac{\partial z}{\partial x} = \mu \frac{V_S}{\kappa} \tag{71}$$

When two phases are present, the situation is quite complex, especially in beds of fine solids where interfacial forces can be significant. In coarse beds, eg, packed towers, the effects are often correlated empirically in terms of pressure drops for the single phases taken individually.

3.8. Non-Newtonian Fluids. For many fluids the Newtonian constitutive relation involving only a single, constant viscosity is inapplicable (2,4,32,33). Either stress depends in a more complex way on strain, or variables other than the instantaneous rate of strain must be taken into account. Such fluids are known collectively as non-Newtonian and are usually subdivided further on the basis of behavior in simple shear flow, ie, flow between sliding planes or, to a good approximation, between two mutually rotating cylinders. Figure 14

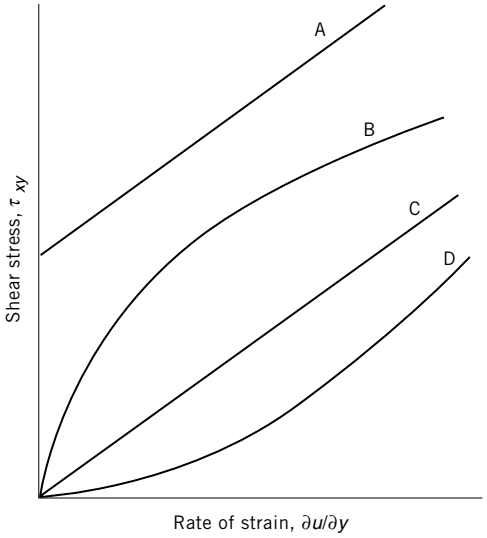

Fig. 14. Fluid behavior in simple shear flow where A is Bingham; B, pseudoplastic; C, Newtonian; and D, dilatant fluid.

illustrates the behavior of several types of the generalized Newtonian fluid. This simple generalization uses the Navier-Stokes equations but takes viscosity to depend in some way on the rate of strain, as described by the constitutive relationship of the fluid.

The behavior of a large class of non-Newtonian fluids can be represented by the power law

$$\tau_{yx} = K\left(\frac{\partial U}{\partial y}\right)^n \tag{72}$$

where K is the consistency index and n is the behavior index, both of which are empirical constants. Fluids with $n < 1$, called pseudoplastic, are the most commonly encountered non-Newtonian fluids. Examples are polymeric solutions, some polymer melts, and suspensions of paper pulps. Their apparent viscosity, defined as $\tau_{yx}/(\frac{\partial U}{\partial y})$, drops with increased rate of strain. Fluids with $n > 1$, called dilatant, have apparent viscosities that increase with increased rate of strain. Dilatancy is observed in highly concentrated suspensions of very small particles such as titanium oxide in a sucrose solution.

Another common class of non-Newtonian fluids is the Bingham fluids, which have a linear constitutive relationship, similar to Newtonian fluids, but have a nonzero intercept termed the yield stress:

$$\tau_{yx} = \tau_{yield} + \mu_o \frac{\partial U}{\partial y} \tag{73}$$

The coefficient μ_o is termed the modulus of rigidity. The viscosities of thixotropic fluids fall with time when subjected to a constant rate of strain, but recover upon

standing. This behavior is associated with the reversible breakdown of structures within the fluid, which are gradually reestablished upon cessation of shear. The smooth spreading of paint following the intense shear of a brush or spray is an example of thixotropic behavior. When viscosity rises with time at constant rate of strain, the fluid is termed rheopectic. This behavior is much less common but is found in some clay suspensions, gypsum suspensions, and certain soils.

When these relatively simple fluids are conveyed in laminar flow in pipes, the behaviors can be deduced directly and quantitatively from constitutive relations and the assumption of linear variation of shear stress with radius. Pseudoplastic fluids display lower viscosities in the high shear region on the wall than at the pipe axis. Their velocity profiles are steeper at the wall and flatter at the axis than the parabolic shape developed by Newtonian fluids. Dilatant fluids show opposite behavior, tending to freeze at the wall and finger along the axis. Bingham fluids show no velocity gradient up to the radius at which the yield stress is reached, giving the impression of a solid core of material moving along the axis. Pipelines conveying thixotropic and rheopectic fluids are usually designed on a most viscous basis. For thixotropic fluids, this corresponds to viscosity at time zero, but for rheopectic fluids the viscosity after extended shear is used.

The pressure drop accompanying pipe flow of non-Newtonian fluids can be described in terms of a generalized Reynolds number. For power-law types, this takes the form:

$$Re_{pl} = \frac{8\rho V^{2-n} D^n}{K[2(3n+1)/n]^n} \tag{74}$$

The transition from laminar to turbulent flow occurs at Reynolds numbers varying from $\sim$2000 for $n \geq 1$ to $\sim$5000 for $n = 0.2$. In the laminar regime, the friction factor, as defined by equation 50, is related to Re_{pl} in a fashion identical to that for Newtonian fluids, ie,

$$f = \frac{64}{Re_{pl}} \tag{75}$$

In the turbulent regime, the friction factor increases significantly with increasing values of n. Its variation is shown in Figure 15.

For Bingham fluids, the corresponding Reynolds number is defined as

$$Re_{Bin} = \frac{\rho VD}{\mu_o} \tag{76}$$

The yield stress is presented in dimensionless form as the Hedstrom number

$$\mathrm{He} = \frac{\tau_{\mathrm{yield}} \mathrm{D}^2 \rho}{\mu_{\mathrm{o}}^2} \tag{77}$$

this parameter is the product of the Bingham number (ie, the ratio of yield stress and viscous stress) and the Reynolds number. Figure 16 shows the variation of

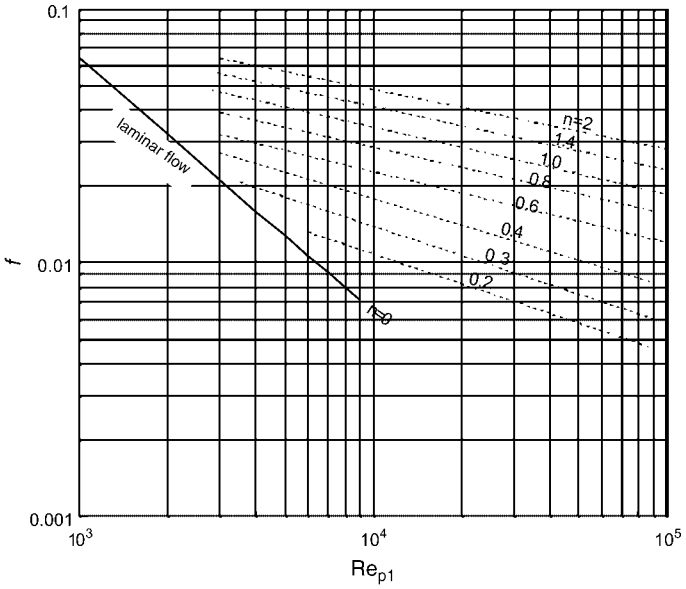

Fig. 15. Friction factor variation for power-law-type fluids [adapted from (2)].

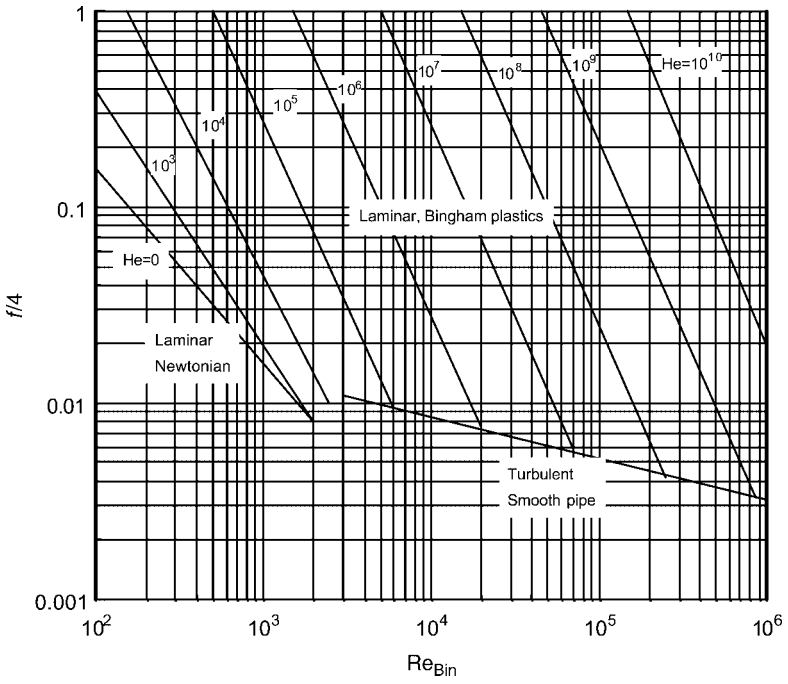

Fig. 16. Friction factor variation for Bingham fluids; notice that $f/4$ is plotted instead of f [adapted from (2)].

the friction factor for Bingham fluids with different values of He. The Reynolds number for transition to turbulence can be found from the same figure as the intersection of the line for turbulent flow in Newtonian fluids and the corresponding constant-He line.

In configurations more complex than pipes, eg, for flow around bodies or through nozzles, additional shearing stresses and velocity gradients must be accounted for. More general equations for some simple fluids in laminar flow are described in Ref. 4.

Many industrially important fluids cannot be described in simple terms. Viscoelastic fluids are prominent offenders. These fluids exhibit memory, flowing when subjected to a stress, but recovering part of their deformation when the stress is removed. Polymer melts and flour dough are typical examples. Both the shear stresses and the normal stresses depend on the history of the fluid. Even the simplest constitutive equations are complex, as exemplified by the Oldroyd expression for shear stress at low shear rates $\gamma\cdot$:

$$\tau + \lambda_1 \frac{d\tau}{dt} = \mu\left(\frac{d\cdot\gamma}{dt} + \lambda_2 \frac{d^2\cdot\gamma}{dt^2}\right) \tag{78}$$

The relaxation times λ_1 and λ_2 describe the times required to relieve stress on the cessation of strain and to relieve strain on the cessation of stress, respectively. The full Oldroyd tensor requires knowledge of eight material properties.

The development of significant normal stresses in such fluids can lead to bizarre behaviors when the fluids are deformed. Stirred viscoelastic fluids can move radially inward and climb the stirring shaft (the Weissenberg effect), if the inward-directed normal stresses accompanying shear are greater than the centrifugal forces developed by the stirring. When viscoelastic polymer melts are extruded through dies, they swell, recovering in part the lateral dimensions they possessed upstream of the die. At some critical rate the polymer undergoes melt fracture. Stress is relieved in an unsymmetrical manner and the extruded rod takes on a screw-like form. As the flow increases, additional modes of instability appear and the rod takes on progressively more complex shapes.

3.9. Two-Phase Flows. *Gas-Liquid Flows.* When two or more fluids flow together, a much greater range of phenomena occurs as compared to flow of a single phase. In a conduit many of the technically significant phenomena have to do with the positions assumed by the phase boundaries, and these are governed by the flow conditions rather than by the walls of the conduit. In addition to the densities and viscosities, surface properties can be important. Methods for quantitative calculation for gas–liquid flow are poorly developed in comparison to those for single-phase flow. Consider, for example, pressure drop for fully developed, steady-state, incompressible flow in smooth conduits. For single-phase flow, dimensional analysis shows that only two dimensionless numbers are involved, the friction factor and the Reynolds number, and a set of experiments in which only two measurable quantities are varied suffices to establish the desired empirical correlation. For fully developed gas–liquid flow in horizontal pipes alone, there are at least six such groups and a six-dimensional space must be mapped. This has not yet been fully accomplished although thousands of experimental measurements have been made. The methods available

run the gamut from empirical correlations only weakly based, if at all, on an understanding of the phenomena, to correlations based on conceptual models that use simplifying relations connecting the variables of the multidimensional problem. Even with the best correlations, however, errors of a factor of two are not uncommon. Much of the data on which available correlations are based are obtained in small-diameter (ie, <100 mm) pipes using air and water. There is still much uncertainty as to how or even whether such data can be extrapolated to large pipes conveying fluids having significantly different properties.

Despite these difficulties, many useful calculations can be made, particularly when the effects of changes in an already existing operation are of interest. All of these calculations depend on an accurate picture of the flow regime, used to denote the significant configurational characteristics of the flow, eg, unidirectional, recirculating, steady, unsteady, liquid-dispersed, gas-dispersed, etc. For illustration, consider the simultaneous flow of air and water at various velocities in a 25-mm horizontal pipe. It is desirable to know such things as which phase is continuous, the degree of dispersion or atomization, and the presence or absence of flow surges. At low velocities, both phases are continuous and flow smoothly and the flow is stratified, as sketched in the lower left-hand corner of Figure 17. As either the liquid-flow rate or gas-flow rate is raised, the flow becomes unstable by a Kelvin-Helmholtz instability. This causes waves to rise at the phase interface, producing wave-stratified flow. With further increase in liquid-flow rate, the waves grow in amplitude, and at some flow rate touch the upper wall of the pipe, destroying the continuity of the gas phase. This is plug flow or slug flow, the former term connoting the more gentle action in which the gas bubble moves forward without intense agitation, and the latter one expressing the more violent action observed at higher gas-flow rates. As liquid-flow rate is raised still further, the gas plugs break up into rather small bubbles. The flow may then be described as bubble flow or froth flow, according to whether the gas volume fraction is small or large, respectively.

If the gas-flow rate is increased, one eventually observes a phase transition for the abovementioned regimes. Coalescence of the gas bubbles becomes important and a regime with both continuous gas and liquid phases is reestablished, this time as a gas-filled core surrounded by a predominantly liquid annular film. Under these conditions, there is usually some gas dispersed as bubbles in the liquid and some liquid dispersed as droplets in the gas. The flow is then annular. Various qualifying adjectives may be added to further characterize this regime. Thus, there are semiannular, pulsing annular, and annular mist regimes. Over a wide variety of flow rates, the annular liquid film covers the entire pipe wall. For very low liquid-flow rates, however, there may be insufficient liquid to wet the entire surface, giving rise to rivulet flow.

At very high flow rates, phenomena occur that are equivalent to the sonic flow observed with gases. This is illustrated in Figure 17 by the envelope labeled choked flow. Without special effort, it is impossible to produce velocities in a pipe at rates higher than indicated by the envelope. It is especially noteworthy that the limiting gas velocity can be very low provided the liquid rate is high. Realization of this fact has often come as a surprise to a designer who has calculated higher velocities in some pipes.

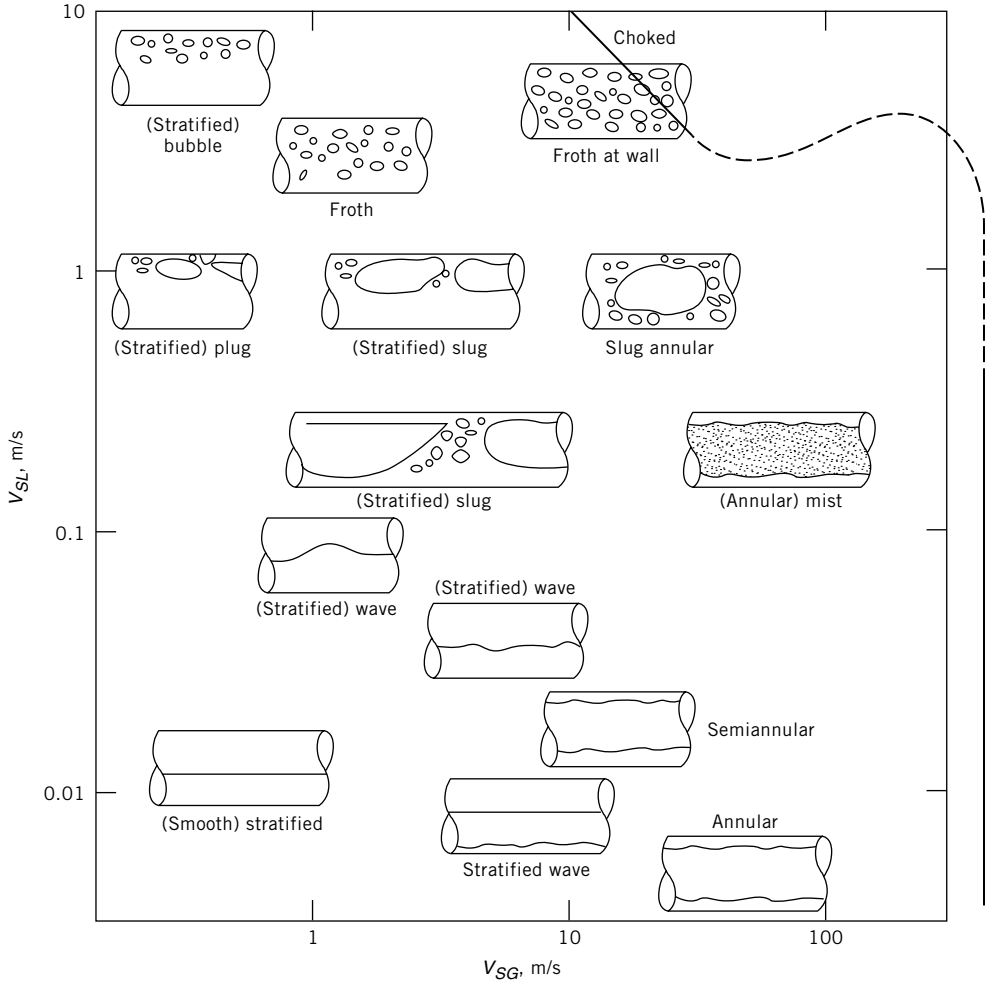

Fig. 17. Flow regimes for air–water in a 2.5-mm horizontal pipe where V_{SL} is superficial liquid velocity and V_{SG} is superficial gas velocity. Courtesy of Shell Development Co.

In inclined or vertical pipes, the flow regimes are similar to those described for horizontal pipes when both gas- and liquid-flow rates are high. At lower flow rates, the effects of gravity are important and the regimes of flow are quite different. For liquid velocities near 0.3 m/s and gas velocities near 1.5 m/s, piston or vertical slug flow is observed (Fig. 18). Large gas bubbles, having approximately spherical top surfaces, bridge the pipe. The calculation of the rate of rise of such bubbles can be made fairly accurately by assuming frictionless flow near the bubble apex. The success of this rather simple calculation illustrates one of the advantages of having a firm knowledge of flow regimes.

The upward flow of gas and liquid in a pipe is subject to an interesting and potentially important instability. As gas flow increases, liquid holdup decreases and frictional losses rise. At low gas velocity the decrease in liquid holdup and

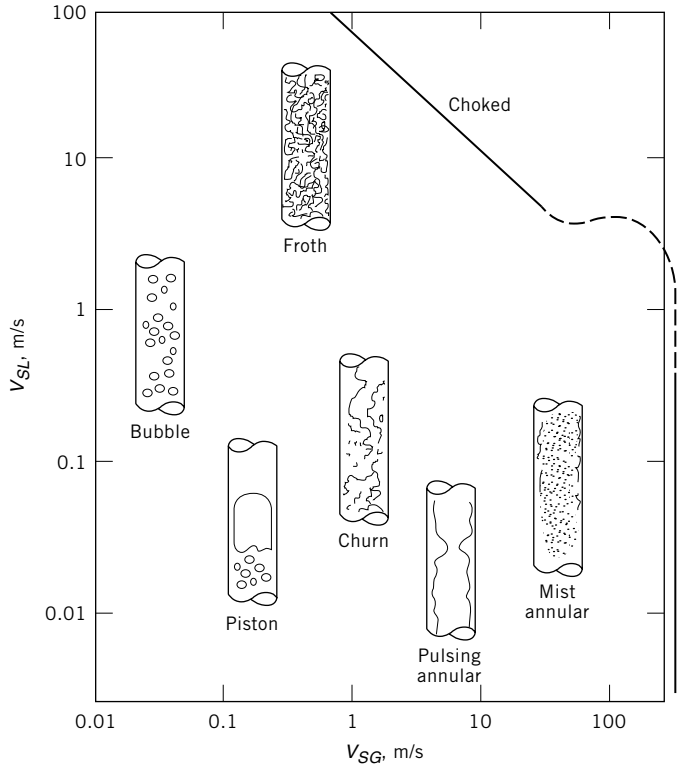

Fig. 18. Flow regimes for air–water in a 25-mm vertical pipe where V_{SL} is superficial liquid velocity and V_{SG} is superficial gas velocity. Courtesy of Shell Development Co.

gravity head more than compensates for the increase in frictional losses. Thus, an increase in gas velocity is accompanied by a decrease in pressure drop along the pipe, which constitutes a potentially unstable situation if the flows of gas and liquid are sensitive to the pressure drop in the pipe. Such a situation can arise in a thermosyphon reboiler, which depends on the difference in density between the liquid and a liquid–vapor mixture to produce circulation. The instability is manifested as cyclic surging of the liquid flow entering the boiler and of the vapor flow leaving it.

Atomization. A gas or liquid may be dispersed into another liquid by the action of shearing or turbulent impact forces that are present in the flow field. The steady-state drop size represents a balance between the fluid forces tending to disrupt the drop and the forces of interfacial tension tending to oppose distortion and breakup. When the flow field is laminar, the ability to disperse is strongly affected by the ratio of viscosities of the two phases. Dispersion, in the sense of droplet formation, does not occur when the viscosity of the dispersed phase significantly exceeds that of the dispersing medium (34).

More commonly, atomization occurs under turbulent conditions. The mechanism of atomization and its quantitative description are still incompletely understood. It is possible that breakup occurs because of the impact forces

exerted by the small, nearly isotropic turbulent eddies (35). The effects of these eddies are measured by the local rate of energy dissipation, but because this quantity is seldom known, correlations are often expressed in terms of average energy dissipation per unit mass or volume. In fact, in most important situations, breakup occurs in highly anisotropic regions, where the local energy dissipation bears little relationship to the average and where nonturbulent mean shearing stresses may be large. For example, in stirred tanks breakup occurs mostly in the vortices shed from the turbine blades. In pipe flow it appears that, at least initially, breakup occurs close to the wall, quite likely as a result of mean flow shear. Drop size is related to velocity gradient and not to average energy dissipation. Under these circumstances, the most practical approach is to employ empirical correlations derived for the geometries and residence times of interest.

Drop or bubble sizes are also strongly affected by the tendency of the drops or bubbles to coalesce once they enter regions of low turbulence or low mean shear. When coalescence is rapid, as in dispersion of gas in pure liquids, average bubble size seems to be determined by the average rate of energy dissipation and is insensitive to how the energy is applied. Correlations obtained for one geometry can be applied with reasonable success to other geometries. In many liquid–liquid systems where coalescence rates are lower, the drops made in the regions of intense shear can persist throughout. In a stirred vessel, eg, these drops are characteristic of conditions near the impeller and the same impeller operating at the same speed in two vessels of different sizes gives about the same size drops, despite the lower average energy dissipation in the larger vessel. In the extreme case of no coalescence, eg, in emulsions stabilized by surface-active agents, drop sizes are determined by the highest shear rates available. In a stirred vessel, this results in a sensitivity of drop size only to tip speed and not to impeller shape or energy input. In a practical situation the time needed to emulsify is as important as ultimate drop size, and impellers providing reasonable circulation times are required.

Flow Past Deformable Bodies. The flow of fluids past deformable surfaces is often important, eg, in flows of liquids containing gas bubbles or drops of another liquid (36). Proper description of the flow must allow for both the deformation of these bodies from their shapes in the absence of flow and for the internal circulations that may be set up within the drops or bubbles in response to the external flow. Deformability is related to the interfacial tension and density difference between the phases; internal circulation is related to the drop viscosity. One would have to consider the material properties of both the continuous phase (indicated by the subscript "c") and the distributed phase (indicated by the subscript "d"). A proper description of the flow involves not only the Reynolds number $\mathrm{Re} = \rho_c V_{rel} D_d/\mu_d$, but also other dimensionless groups, including the viscosity ratio, μ_d/μ_c, the Eötvos number $\mathrm{Eö} = g\ (\rho_c - \rho_d)\ D^2_{drop}/\sigma$ and the Morton number $\mathrm{Mo} = g\mu_c^4\ (\rho_c - \rho_d)/\rho_c^2\sigma^3$.

Where surface-active agents are present, the notion of surface tension and the description of the phenomena become more complex. As fluid flows past a circulating drop (bubble), fresh surface is created continuously at the nose of the drop. This fresh surface can have a different concentration of agent, hence a different surface tension, from the surface further downstream that was created earlier. Neither of these values need equal the surface tension developed in a

static, equilibrium situation. A proper description of the flow under these circumstances involves additional dimensionless groups related to the concentrations and diffusivities of the surface-active agents.

Because of high buoyancy and frequently large size, gas bubbles rising in a liquid can deviate greatly from spherical shapes. Figure 19 illustrates the behavior observed. In pure liquids small bubbles rise faster than would be predicted from the drag correlations developed for solid spheres, because internal circulation permits a higher fluid velocity at the surface and less drag than for the

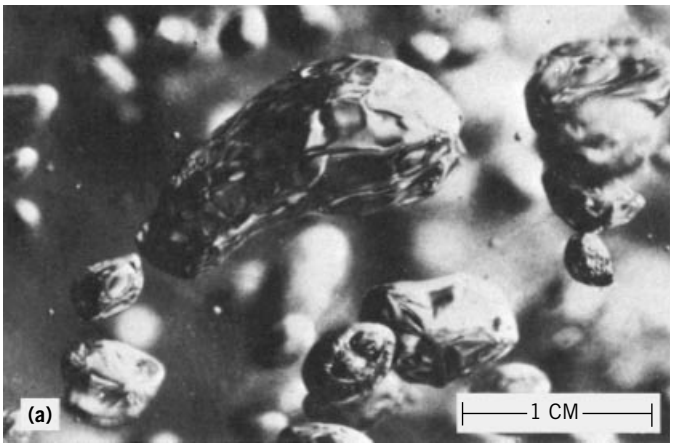

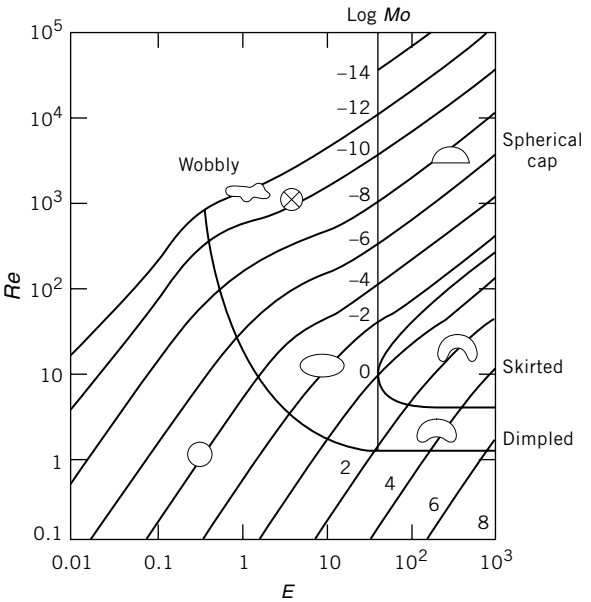

Fig. 19. Shapes of drops and bubbles. (**a**) Bubbles rising in sparged tower system: air–water. Courtesy of Shell Development Co. (**b**) Bubble and droplet regimes, where— represents a 5-mm gas bubble rising in water at 20°C (36).

corresponding solid. Very large bubbles rise much more slowly than do undeformed spheres of the same volume. This is caused by deformation to a shape of large frontal area but small thickness. Very small bubbles obey Stokes law for solid (immobile) surfaces. This behavior is reflected also in the mass-transfer coefficients for such bubbles, which are lower than would be expected from the correlations developed for larger, circulating bubbles.

4. Computational Fluid Dynamics

Analytical solutions of the equations of motion are known only for a small number of laminar and inviscid flows in fairly simple geometrical configurations subjected to well defined boundary and/or initial conditions. The fact that the majority of problems of practical interest are not amenable to such "exact" solutions has motivated the development of powerful numerical algorithms for their computation. The various methods of numerical solutions of fluid mechanical and related equations are collectively known as computational fluid dynamics (CFD). The field of computational fluid dynamics is moderately mature. A vast repertoire of techniques exists and solutions to many complex flows directly relevant to industrial situations can be obtained. Also, a number of reliable CFD codes are commercially available. Although at the research level and for large-scale industrial computations the need for supercomputers or large clusters of parallel processors remains keen, many engineering problems can be solved with acceptable accuracy using personal computers. Future advances in computer speed, code parallellization and new algorithm development promise further improvements in CFD capabilities.

The start of all numerical procedures is the identification of appropriate equations, usually partial differential equations, but also algebraic, ordinary differential or integral, which describe the physical problem at hand. The continuity and momentum equations are the most common, sometimes supplemented by the energy equation, constitutive relationships, empirical correlations and models and equations describing additional physical phenomena in interaction with the flow, such as scalar transport, chemical and biochemical reactions, phase changes and electromagnetic fields and motion/deformation of solid boundaries and interfaces. Appropriate boundary and initial conditions must be also specified and the set of equations and associated conditions must be known to constitute a well-posed mathematical problem, namely, one that is solvable, at least in principle. A counterexample presented earlier is the Reynolds equations for turbulent flows, which contain more unknowns than the available number of equations.

The next step is to convert the equations into forms that can be solved digitally. This usually entails the discretization of both the differential equations and the space–time domain of interest. The flow domain is divided into a network of discrete elements and the pertinent differential equations are replaced by a set of linear algebraic equations for the unknown dependent values at the discrete elements, rather than in continuous space. Time, if a factor, is discretized into time steps. The set of algebraic equations is then solved using highly efficient numerical algorithms to provide values of the dependent variables, such as velocity,

pressure, temperature, etc, at the discrete elements and at the specified time steps.

Among the techniques available for the discretization of the partial differential equation set, commonly used are finite-difference (FDM), finite-volume (FVM), finite-element (FEM), and spectral methods. The finite-volume method is the most widely used method in the CFD codes utilized by the process industries. In the FVM, each partial differential equation is replaced by a set of algebraic finite-difference equations obtained by integration over a fictitious control volume surrounding the point of location of the relevant variable in the mesh structure.

CFD has reached a level of development that it can produce reliable simulations of many fluid mechanical problems of interest in chemical processes, particularly for laminar viscous flows. Even so, it still faces significant challenges, which include the simulation of complex turbulent flows, flows interacting with moving and deformable solid boundaries and free surfaces, multiphysics and multiphase flows, and flows with phase change and chemical reactions. Some of these difficulties are associated with an inadequate understanding and modeling of the related processes, while others are entirely attributed to speed and memory limitations of available computers. Reflecting the fact that the majority of flows of technological interest are turbulent, significant effort has been put into the development of turbulent flow numerical simulation methods. Such methods will be briefly discussed below.

Computation of Turbulent Flows. The time-dependent, three-dimensional Navier-Stokes equations are generally considered adequate to represent turbulent flows and so their solutions, which would be functions of location and time, should be realistic (18,37). CFD analyses that produce such solutions are called Direct Numerical Simulations (DNS) (38) and require the use of a mesh and time step that are fine enough to resolve the smallest motions of dynamic significance (ie, comparable to the so called Kolmogorov microscale and time scale, respectively). At the same time, the computational domain has to be maintained large enough to encompass the large-scale features of the flow and the integration time large enough for the solution to become insensitive to the applied starting conditions. As the flow Reynolds number increases, however, the fine structure of the turbulence becomes increasingly finer, thus requiring a finer mesh for its simulation. As a result, DNS have only been performed successfully mainly on relatively low Reynolds number flows with relatively simple geometrical boundaries, including, among others, homogeneous and isotropic turbulence, boundary layers, channel flows, and isothermal and chemically reacting mixing layers. As algorithms and computers improve, DNS will be able to tackle a wider range of problems, but it is clear that full-scale simulations of large technological systems, such as flying aircraft and turbomachinery, will remain indefinitely beyond DNS capabilities. For the time being, DNS is recognized for its significant contributions to our understanding of turbulence fundamentals, particularly the fine structure and mixing mechanisms of turbulence.

An alternative approach, far less computationally intensive than DNS, but also based on the unsteady Navier-Stokes equations, is offered by Large Eddy Simulations (LES) (39,40). The mesh in these simulations is fine enough to describe the large scale motions and part of the activity in the intermediate,

"inertial" subrange, but too coarse to precisely resolve the finest motions of turbulence, where most of the kinetic energy dissipation to heat takes place and where mixing my molecular motions occurs. LES model the fine structure through a subgrid scale model and incorporate this model into a set of spatially filtered dynamic equations, which are then solved numerically. The simplest and most popular subgrid scale model is the Smagorinsky model, which is based on the eddy viscosity concept (see below), but more complex and versatile models have also been suggested (41). LES have met with significant successes in simulations of atmospheric and laboratory turbulence, particularly the identification of coherent structures that are often responsible for large-scale transport and mixing. Nevertheless, and despite early expectations, LES have not yet developed to an all-purpose numerical tool for flows of engineering interest.

Thus, the most economical and effective engineering analyses of turbulent flows are still based on the earlier approach of developing closure schemes, called turbulence models, allowing the solution of statistically averaged equations. This approach is generally known as RANS (Reynolds-averaged Navier-Stokes) simulations (42,43). A large number of closure models are based on the Boussinesq concept of eddy viscosity, which models the turbulent shear stress as proportional to the mean strain rate (gradient transport), by analogy to the viscous shear stress in Newtonian fluids, which is proportional to the stain rate. For a flow dominated by mean shear in the x_1-direction, the Boussinesq approximation is

$$-\rho\langle u_1 u_2\rangle = \mu_T \frac{\partial\langle U_1\rangle}{\partial x_2} \tag{79}$$

where μ_T, or more commonly, $\nu_T = \mu_T/\rho$ is the eddy viscosity. Unlike the fluid viscosity μ and kinematic viscosity $\nu = \mu/\rho$, which are material properties, the eddy viscosity is a flow property and depends strongly on the local turbulence. Dimensionally, the eddy viscosity ν_T may be considered as the product of a characteristic length scale and a characteristic velocity scale of the local turbulence, and so the determination of ν_T is reduced to the determination of suitable characteristic scales. Thus, eddy viscosity models are usually categorized according to the number of supplementary transport equations which must be solved to supply these scales or equivalent parameters. The so-called zero-equation models do not use any additional equations but empirical information specific to each flow configuration. The best known example is the Prandtl mixing length hypothesis, providing the eddy viscosity as:

$$\nu_T = l_M^2 \left|\frac{\partial\langle U_1\rangle}{\partial x_2}\right| \tag{80}$$

where l_M, the mixing length of turbulent motion, must be specified. The model gives good predictions for many boundary layers, in which case l_M is taken to be proportional to the distance from the wall, and thin shear layer flows, in which case l_M is taken to be proportional to the width of the turbulent region. However, equation 80 assumes that turbulence production is equal to the dissipation at each point in the flow field, a deficiency leading to unrealistic

simulations in many cases. Early one-equation models have fallen in disuse and the only one in current use is the Spalart-Allmaras model, which introduces a modeled transport equation for the eddy viscosity and has found application mostly in external flows. The most popular turbulence models, combining versatility and reasonably low computational times, are two-equation models that supplement the RANS equations with two additional differential equations. These include the k-ε model, which utilizes transport equations for the turbulent inetic energy per unit mass

$$k = \frac{1}{2}\sum_{i=1}^{3}\langle u_i^2\rangle \tag{81}$$

and its rate of dissipation by friction ε, and the k-ω model, which utilizes transport equations for k and the specific dissipation rate (an inverse time scale) $\omega \propto \varepsilon/k$. The k-equation is derived following the Reynolds procedure from the Navier-Stokes equations. It relates the rate of change of k to the advective transport by the mean motion, turbulent transport by diffusion, generation by interaction of turbulent stresses and mean velocity gradients, and dissipation. Equations for ε and ω are devised by analogy to the k-equation and not from first principles. All these equations rely heavily on modeling of the unknown terms, utilizing gradient transport concepts repeatedly. The k-ε model has been used very widely in both commercial and home made codes and found reasonable success in a wide variety of applications. Among its known limitations is the computation of swirling and curved flows and relatively low Reynolds number flows, especially close to a wall. Improved performance in such cases has been achieved by a variant known as the RNG (Renormalization Group) k-ε model. In addition, empirical relations called wall functions are used to bridge the viscous sublayer.

An inherent limitation of eddy-viscosity based models is that they model turbulence as isotropic, giving all turbulent stresses as

$$-\rho\langle u_i u_j\rangle = \mu_T\left(\frac{\partial\langle U_i\rangle}{\partial x_j} + \frac{\partial\langle U_j\rangle}{\partial x_i}\right) - \frac{2}{3}\rho k\delta_{ij} \tag{82}$$

(Kronecker's delta δ_{ij} is equal to 1 when $i = j$ and 0 otherwise), which is a generalization of equation 79. Reynolds stress models (RSM) do not assume this relationship, but instead introduce additional differential transport equations for the individual stresses $-\rho\ \langle u_i u_j\rangle$. These transport equations are often referred to as second-order closure schemes and are solved simultaneously with the modeled dissipation equation and the Reynolds averaged equations. Thus RSM models require more computer time and memory because of the larger number of equations involved and the nonlinearity and strong coupling of the set of equations. This extra effort, however, yields more realistic results for flows having rotation, curvature, and strong swirl. Simplified relations in the form of eddy viscosity equations have been used to model the convective and diffusive terms in the differential stress transport equations, thus reducing them to algebraic expressions. These simplified models, which retain many of the features of the RSM models, are called algebraic stress models (ASM).

The current trend in turbulent modeling is not to produce more complex models, but rather to refine relatively simple models to achieve an acceptable compromise between accuracy and economy of computation. In this respect, attention is given to the approach known as Unsteady RANS (URANS) (44), which contains features of conventional RANS and LES. In this method, the mesh is finer than that in conventional RANS but substantially coarser than would be required for LES. URANS employs turbulent models but also resolves the time-dependent large-scale motions and the total turbulent activity can be found by adding the corresponding local solutions of the equations and the time averaged fluctuations.

5. Experimental Fluid Mechanics

Despite significant developments in CFD, experimental fluid mechanics remain an indispensable source of practical information for designing engineering systems and solving engineering problems as well as a prerequisite in developing and verifying theories, models and algorithms. Much of our understanding of physical phenomena and mechanisms and the discovery of new concepts and applications is based on ingeniously conceived and meticulously executed experiments. Measurements of fluid mechanical properties are performed regularly on actual technological, biological and environmental systems, in order to monitor or control their performance. Such systems may also be used to perform experiments designed to expand our knowledge of associated phenomena and accumulate information which can be used in designing and optimizing future components. Quite commonly, however, experimental fluid mechanics utilize laboratory-based apparatus, which in some way simulates the actual or idealized performance of real systems. Among the most commonly used laboratory apparatus are wind tunnels, water tunnels, open channels, towing tanks and flow loops of various designs using different kinds of liquids and gases or multi-phase materials. Sometimes the objective of measurement is to document bulk properties, namely values averaged in space and/or time, as, eg, the flow rate of and average pressure drop in a fluid flowing through a pipe or the average drag force on an object immersed in highly turbulent flow. Other times, however, the interest is in measuring temporal variations of a property at a specific location, and even the simultaneous temporal variation of local properties throughout the flow domain. It is obvious then that requirements on the response of instrumentation and measuring procedures vary widely, according to the objectives of each experiment.

The remainder of this section briefly outlines the main types of instrumentation and experimental methods used for the measurement of pressure, flow velocity, temperature and related properties. Much more descriptive discussions of these topics can be found in general references (45–55). The reader's attention is also directed to references discussing the related topics of signal acquisition and processing (56) and measurement uncertainty (57,58).

Measurement of Flow Rate. This area encompasses the various flow meters which measure either the mass or the volumetric flow rate through the cross-section of a pipe, duct, etc (59–61). They include:

Direct methods, which essentially time the passage of a given mass or volume of the fluid. The simplest direct method, suitable for liquids only, is to collect the discharge in a container of known volume. Positive displacement flow meters perform the same task but operate continuously in line with the flow circuit. They isolate an amount of fluid entering into them within a well-defined compartment and then discharge it to their outlet. Representative types of positive displacement flow meters for liquids are nutating disk, reciprocating piston, rotary piston, rotary vane, and rotor types; for gases, they are roots, diaphragm and liquid-sealed drum types.

Restriction flow meters, which impose a restriction to the flow and thus introduce a pressure difference, from which one can determine the flow rate by using either a physical principle (eg, Bernoulli's equation) or an empirical calibration. Most common for pipe flows are the Venturi, nozzle, and orifice-plate flow meters. For open channel flows, common are weirs and various flumes, including the Venturi, Parshall and Palmer-Bowlus flumes.

Averaging Pitot-tubes, which are transverse tubes spanning the cross-section and having multiple orifices facing the flow so that they average the total pressure across the flow.

Laminar flow elements, which contain honeycombs or tube bundles with sufficiently narrow individual cross-sections for the flow through each element to be laminar and so they take advantage of the linear relationship between the pressure difference across them and the flow rate.

Rotameters or variable area flow meters, which direct the flow upwards through a vertical tapered tube containing a sphere, cone or other specially shaped bluff body; the flow rate is indicated by the vertical position of the body, in correspondence to the drag force it experiences.

Vortex shedding flow meters, which provide the bulk velocity through its relationship to the frequency of vortices shed by an immersed bluff body with sharp edges.

Drag or target flow meters, which determine the bulk velocity from the measured drag force on a disk or other object, called the target.

Turbine flow meters, which include axial turbines and paddlewheels and provide the flow rate from its relationship to the speed of rotation of the impeller.

Ultrasonic flow meters, which transmit ultrasound across the flow and either measure its Doppler shift by dispersed scattering particles, or the difference in transmission times of sound propagating toward upstream and downstream.

Electromagnetic flow meters, which are suitable for electrically conducting liquids in pipes and measure the flow rate from a voltage difference across the pipe caused by electric charge motion in an imposed magnetic field.

Coriolis flow meters, which pass the fluid through an oscillating element and utilize the Coriolis effect; they are true mass flow meters and suitable for non-Newtonian and multiphase flows.

Thermal mass flow meters, suitable for gas flows and monitoring temperature differences introduced to the stream by heating elements; they require calibration and correction factors when used in gases of different properties.

Criteria for the selection of a flow meter include cost, range of operation, accuracy, suitability for the particular flow of interest and pressure losses imposed on the flow. A large variety of such instruments are available from many different manufacturers.

Pressure Measurement. Pressure measurement in fluids is of great interest in many engineering applications, due to the relationship of pressure to flow velocity and forces on objects. Among the most common pressure-measuring instruments one could list the following:

Liquid-in-glass manometers, either vertical or inclined, including various micromanometers.

Mechanical pressure gages, including deadweight gages and Bourdon-tube types, which deform under pressure.

Electrical transducers, including piezoelectric, strain-gage and variable capacitance, reluctance and inductance types; more recent types include semiconductor and microelectromechanical (MEMS) transducers.

In many cases, pressure is measured at the wall, through a small pressure tap or by mounting the transducer flush with the flow. To measure in-flow pressure, one may introduce a thin tube, which, depending on its design, can measure the static (static tube) or the impact (Pitot tube) pressure. Fast response probes utilize pressure transducers within the pressure tubes. Wall pressure variation can be mapped with pressure sensitive paints, a technique used mostly in aerodynamics experiments.

Temperature Measurement. The most common types of thermometers are

Liquid-in-glass thermometers, which contain mercury, alcohol or another liquid and measure temperature from the thermal expansion of the liquid. They are classified into complete, total and partial immersion types.

Bimaterial thermometers, mostly bimetallic, but also utilizing semiconductors. They consist of two thin, bonded together, layers of materials with drastically different thermal expansion coefficients, which deform when exposed to different temperatures. The alloy Invar is frequently used, due to its extremely low thermal expansion coefficient.

Thermocouples, which are pairs of junctions of two metals that generate a voltage difference when exposed to different temperatures (Seebeck effect). Common are the J, E and K types.

Resistance temperature detectors (RTD), which measure temperature through changes of the electrical resistance of a metallic element, usually made of platinum or nickel. Very fine (1-μm diameter) platinum wires (cold wires) are used for measuring temperature fluctuations in turbulent air streams up to frequencies of a few kHz.

Thermistors, which are semiconductor resistance thermometers. They are very sensitive, compared to RTD and thermocouples, but also highly nonlinear and usable mainly in temperatures not very far from the ambient value.

High temperatures, above a few thousand degrees, can only be measured by radiation emission methods, using optical pyrometers. Surface temperatures can also be monitored using infrared thermography, while surface temperature maps can be obtained with the use of temperature sensitive paints and liquid crystals. Additional temperature measurement methods include laser-induced fluorescence and interferometry.

Velocity Measurement. Unlike flow rate measurement methods, local flow velocity measurement entails sufficient spatial resolution to essentially identify the velocity at a particular location and often to map the velocity variation over a line, surface or volume of interest. Some velocity measurement methods have relatively slow response and provide time-averaged values, while others have sufficient temporal resolution to measure the instantaneous velocity, as required for the documentation of transient and turbulent flows. The following are the most widely used techniques:

Pressure tubes, mainly combinations of static and Pitot (impact) tubes, which measure velocity from pressure differences. Multihole probes are used to measure velocity in both magnitude and direction, following proper calibration.

Hot wire and hot film anemometry (HWA) (62–64), which measures flow velocity from its cooling effect on electrically heated thin wires (typically 5 μm in diameter) and other fine sensors. Hot wires can only be used in clean gases, but hot films are also suitable for liquid flows. These sensors have the highest temporal resolution among other techniques. Multisensor combinations can be used to measure two velocity components or the entire velocity vector and multiprobe arrangements to provide simultaneous measurements at many locations.

Laser Doppler velocimetry (LDV or LDA) (65–68), which measures the velocity of suspended fine particles through the Doppler shift of laser light scattered by them. Due to the high cost of LDV components, this is essentially a single-point measurement method. Another instrument utilizing the same principle is the ultrasonic Doppler velocimeter, which uses ultrasonic waves, rather than light waves. Its advantage is that it is suitable for opaque fluids, which would obstruct transmission of light.

Particle tracking, which is direct tracing of the positions of suspended particles, by direct viewing or from recorded images. Obviously, this method is impractical when the particle concentration is so high that individual particles cannot be discriminated.

Particle image velocimetry (PIV) (69–71), which, like the previous method, computes velocity from particle displacements, with the difference that such displacements are averaged over a very small interrogation volume and so PIV requires high particle densities. A dual-tube pulsed laser, in combination with a lens that produces a light sheet, are most often used to illuminate two closely timed images of a flow cross-section. A significant advantage of PIV over previous methods is that it can map velocity variation over a planar region, from which one may determine streamlines, vorticity and other properties, as well as instantaneous flow patterns. Its

disadvantage is a relatively low temporal resolution, which is being improved with the development of high repetition-rate pulsed lasers.

Wind velocity is commonly measured with the use of mechanical transducers, including the vane, cup and propeller anemometers (72).

Composition Measurement. The identification of chemical composition of passive mixtures as well as of reacting flows is a very important task in chemical processes and combustion (73,74). When temporal resolution is not of concern, this can be done by isolating a sample of the fluid through a syringe, sampling tube, etc, and then analyzing its composition with the use of an Orsat analyzer, gas chromatography, electronic testers, mass spectrometry, or absorption spectrophotometry. Monitoring of the emissions of exhaust gases from industrial stacks is done with the use of continuous emission monitors (CEM), which are standardized and regulated devices. At the laboratory level, concentration can be measured with reasonable spatial and temporal resolution by the following techniques:

Thermal probes, which are fine heated sensors, sensitive to temperature and velocity, besides concentration and require elaborate calibration. Conductivity probes eliminate the dependence on velocity by passing flow samples through a choked sonic nozzle.

Electric conductivity probes, usable for liquid solutions of electrolytes.

Light scattering methods, which include a variety of techniques. In the simplest case, concentration of smoke and other suspensions can be determined by measuring light absorption along the path of a beam or within a small measuring volume. The Rayleigh scattering method is suitable for binary gas mixtures, while Raman scattering methods can identify both the composition of gas mixtures as well as the concentrations of the constituents.

Laser induced fluorescence methods, which include methods using fluorescent dyes (Fluorescein disodium and Rhodamines) in liquids and fluorescent additives or products or reaction in gases.

The measurement of suspended particulate (solid particles or droplets) can be obtained by gravimetric analysis of samples removed from the suspension and by photographic, visual, and optical methods. Phase Doppler particle analysis is a popular method that provides the size distribution of suspended particles and which can be easily combined with laser Doppler velocimetry to measure simultaneously particle size and local flow velocity.

Void fraction measurement is particularly important in thermonuclear power generation plants. Among the available techniques, one can mention the quick-closing valve method, various sampling methods that separate phases, electric impedance meters, methods based on heat transfer from fine heaters, and methods based on light scattering, ultrasound scattering and X- and gamma-ray radiation absorption.

Flow Visualization. Although of qualitative nature, flow visualization is a very useful component in any fluid mechanics experiment, as it can detect the presence of apparatus malfunctions and unwanted influences, identify the state

of the flow (eg, whether laminar or turbulent) and the boundaries of different flow regions, and provide valuable insight into physical and chemical mechanisms that may affect the flow (75–79). Because motions in clean air, water and many other fluids are cannot be discriminated by the unaided human eye, the visualization of flow patterns requires either the introduction of foreign substances, which act as flow markers when properly illuminated, or the use of optical techniques, which are sensitive to refractive index variations in the fluid. Flow markers for liquids include: tufts, namely, short pieces of flexible yarn, attached to the surface or to thin supports extending mid-stream; dyes of different kinds, either injected into the fluid or locally generated by electrochemical or photochemical reactions; hydrogen bubbles, generated on thin wires by electrolysis of water; air bubbles; and dispersed solid particles (eg, metallic or ceramic dusts or flakes) and droplets of immiscible liquids. Flow markers for gases include: tufts; oil films and dots applied to a surface; sublimating or soluble surface films; pressure and temperature sensitive paints and liquid crystals; smoke produced by burning of different substances and oil mists produced by evaporation/condensation; aerosols; dispersed solid particles; soap bubbles; and sparks. Optical techniques include the shadowgraph technique, the Schlieren technique, interferometry, holography, and streaming birefringence.

6. Nomenclature

A	cross-sectional area, frontal area
B	volume
Ca	capillary number
C_D	drag coefficient
c	concentration, speed of sound
c_i	concentration of species i
c_p	specific heat under constant pressure
D	diameter, frontal height
D_{drop}	droplet diameter
D_h	hydraulic diameter
d_p	particle diameter
$d_{p,av}$	average (Sauter) particle diameter
Eö	Eötvos number
Eu	Euler number
e	roughness height, specific energy
e_{ij}	rate of strain tensor
$\vec{F}_B$	body force vector
F_D	drag force
F_n	normal force component
Fr	Froude number
$\vec{F}_S$	surface force vector
F_t	shear (tangential) force component
f	frequency, friction factor
f_i	body force per unit volume

f_{por}	friction factor for porous media
Gr	Grashof number
g	gravitational acceleration magnitude
g^*	dimensionless gravitational acceleration
g_i	gravitational acceleration vector, $i = 1,2,3$
He	Hedstrom number
h	vertical elevation, overall heat transfer coefficient
J_i	diffusive flux of species i
K	consistency index
Kn	Knudsen number
k	thermal conductivity, turbulent kinetic energy
L	characteristic length
L_{ent}	pipe entrance length
L_o	length scale
l_M	mixing length
M	Mach number
Ma	Marangoni number
Mo	Morton number
Nu	Nusselt number
n	behavior index
P	pressure, wetted perimeter
P^*	dimensionless pressure
P_o	reference pressure
Pr	Prandtl number
P_v	vapor pressure
p	mean-free pressure fluctuation
$\bullet\ Q$	heat transfer rate
R_1,R_2	principal radii of curvature
Ra	Rayleigh number
Re	Reynolds number
Re_{Bin}	Reynolds number for Bingham fluids
Re_{pl}	Reynolds number for power-law fluids
Re_{por}	Reynolds number for porous media
$\mathrm{Re}_{transition}$	transition Reynolds number
Ri	Richardson number
R_i	production rate of species i
Ro	Rossby number
S	surface, surface area
Sc	Schmidt number
St	Strouhal number
T	temperature, time interval
Ta	Taylor number
t	time
U_b	bulk velocity
U_i	velocity vector in Cartesian form, $i = 1,2,3$
U_i^*	dimensionless velocity vector, $i = 1,2,3$
u	specific internal energy
u_i	mean-free velocity fluctuation vector, $i = 1,2,3$

V	velocity magnitude
$\vec{V}$	velocity vector
V_l	interstitial velocity
V_o	velocity scale
V_{rel}	relative velocity
V_S	superficial velocity
$\bullet\ W_{other}$	electrochemical/radiation power
$\bullet\ W_{sh}$	mechanical power by shear stresses
x	streamwise coordinate
x_i	Cartesian coordinate, $i = 1,2,3$
x_i^*	dimensionless Cartesian coordinate, $i = 1,2,3$
y	transverse coordinate
γ	ratio of specific heats, thermal diffusivity
$\bullet\ \gamma$	shear rate
γ_c	molecular diffusivity
ΔP	pressure difference
ΔT	temperature difference
$\Delta V_{\max}$	maximum velocity difference in a free shear flow
δ_{ij}	Kronecker's delta
ε	porosity, void fraction
ε	turbulent kinetic energy dissipation rate
$\vec{\zeta}$	vorticity vector
θ	angle
κ	permeability
λ	molecular mean free path, dilatational viscosity
λ_1, λ_2	relaxation times
μ	(dynamic, shear) viscosity
μ_o	modulus of rigidity
μ_l	liquid viscosity
μ_T	eddy viscosity
ν	kinematic viscosity
ν_T	eddy (kinematic) viscosity
π	3.14149...
ρ	density
ρ_l	liquid density
σ	surface tension, normal stress
σ_c	cavitation number
σ_i	normal stresses, $i = 1,2,3$
τ	shear stress
τ_{ij}	shear stresses, $i, j = 1,2,3$
τ_{xy}	shear stress
τ_{yield}	yield stress
ϕ	velocity potential
ψ	stream function
Ω	rotation rate
$\langle \ldots \rangle$	ensemble average
$(\ldots)$	time average

BIBLIOGRAPHY

"Principles" under "Fluid Mechanics" in *ECT* 1st ed., Vol. 6, pp. 614–640, by T. Baron, University of Illinois, and M. Souders, Jr., Shell Development Co.; "Flow Measurement" under "Fluid Mechanics" in *ECT* 1st ed. Vol. 6, pp. 640–648, by M. Souders, Jr., Shell Development Co.; "Principles" under "Fluid Mechanics" in *ECT* 2nd ed., Vol. 9, pp. 445–473, by M. Souders, Chemical Engineer; "Flow Measurement" under "Fluid Mechanics" in *ECT* 2nd ed., Vol. 9, pp. 473–483, by M. Souders, Chemical Engineer; "Fluid Mechanics" in *ECT* 3rd ed., Vol. 10, pp. 582–629, by A. M. Benson, G. Q. Martin, J. S. Son, and C. V. Sternling, Shell Development Co.; in *ECT* 4th ed., Vol. 11, pp. 171–226, by J. S. Son, Shell Development, "Fluid Mechanics" in *ECT* (online), posting date: December 4, 2000, by J. S. Son, Shell Development.

CITED PUBLICATIONS

1. R. W. Fox, A. T. McDonald, and P. J. Pritchard, *Introduction to Fluid Mechanics*, John Wiley & Sons, Hoboken, New Jersey, 2004.
2. Noel De Nevers, *Fluid Mechanics for Chemical Engineers*, 3rd ed., McGraw-Hill, Boston, 2005.
3. J. O. Wilkes, *Fluid Mechanics for Chemical Engineers*, Prentice Hall, Upper Saddle River, N. J., 1999.
4. R. B. Bird, W. E. Stewart, and E. N. Lightfoot, *Transport Phenomena*, John Wiley & Sons, Inc., New York, 2002.
5. G. K. Batchelor, *An Introduction to Fluid Dynamics*, Cambridge University Press, Cambridge, U.K., 1970.
6. R. D. Blevins, *Applied Fluid Dynamics Handbook*, Van Nostrand Reinhold Company, New York, 1984.
7. S. Goldstein, ed., *Modern Developments in Fluid Dynamics*, Dover Publications Inc., New York, 1965.
8. E. F. Brater and H. W. King, *Handbook of Hydraulics*, 6th ed., Mc Graw-Hill, New York, 1976.
9. R. L. Panton, *Incompressible Flow*, John Wiley & Sons, New York, 1984.
10. S. P. Parker, ed., *Fluid Mechanics Source Book*, McGraw-Hill, New York, 1987.
11. J. Saleh, ed., *Fluid Flow Handbook*, McGraw-Hill, New York, 2002.
12. F. M. White, *Viscous Fluid Flow*, 2nd ed., McGraw-Hill, New York, 1991.
13. F. M. White, *Fluid Mechanics*, 5th ed., McGraw-Hill, New York, 2003.
14. R. W. Johnson, ed., *The Handbook of Fluid Dynamics*, CRC Press, Boca Raton, 1998.
15. S. H. Davis and T. J. Pedley, *J. Fluid Mech.*
16. S. Tavoularis, in E. R. Cohen, D. R. Lide, and G. L. Trigg, ed., *"Fluid dynamics,"* AIP Physics Desk Reference, Springer, New York, 2003, pp. 425–443.
17. J. O. Hinze, *Turbulence*, 2nd ed., McGraw-Hill, New York, 1975.
18. S. B. Pope, *Turbulent Flows*, Cambridge University Press, Cambridge, 2000.
19. S. Tavoularis, in J. M. Saleh, ed., *"Turbulent Flow,"* Fluid Flow Handbook, Chapter 31, McGraw-Hill, New York, 2002, pp. 31.1–31.33.
20. L. Prandtl, Ueber Fluessigkeitsbewegung bei sehr kleiner reibung. Proceedings Third Intern, Mathematics Congress, Heidelberg, Germany, 1904.
21. L. Rosenhead, ed., *Laminar Boundary Layers*, Oxford University Press, Oxford, U.K., 1963.
22. H. Schlichting, *Boundary Layer Theory*, 7th ed., McGraw-Hill, New York, 1979.
23. U. Fey, M. Koenig, and H. Eckelmann, *Phys. Fluids* **10**, 1547 (1998).
24. H. Tennekes and J. L. Lumley, *A First Course in Turbulence*, The MIT Press, Cambridge, Mass., 1972.
25. K. Wark and C. F. Warner, *Air Pollution*, 2nd ed., Harper and Row, New York, 1981.

26. J. M. Beer and N. A. Chigier, *Combustion Aerodynamics*, John Wiley & Sons, Inc., New York, 1972.
27. J. Walker, *Sci. Am.* **238**, 168 (1978).
28. S. Tavoularis, in J. M. Saleh, ed., *Fluid Flow Handbook, "Flow Past immersed objects,"* Chapter 20, McGraw-Hill, New York, 2002, pp. 20.1–20.44.
29. S. A. Thorpe, *J. Fluid Mech.* **46**, 299 (1971).
30. D. Coles *J. Fluid Mech.* **21**, 385 (1965).
31. R. A. Mugele and H. D. Evans, *Ind. Eng. Chem.* **43**, 1317 (1951).
32. W. R. Schowalter, *Mechanics of Non-Newtonian Fluids*, Pergamon Press, New York, 1978.
33. R. I. Tanner, *Engineering Rheology*, Clarendon Press, Oxford, U.K., 1985.
34. H. J. Karam and J. C. Bellinger, *Ind. Eng. Chem. Fundam.* **7**, 567 (1967).
35. V. G. Levich, *Physicochemical Hydrodynamics*, Prentice-Hall, Englewood Cliffs, New Jersey, 1962.
36. J. R. Grace, T. Waigeri, and T. H. Nguyen, *Trans. Inst. Chem. Eng.* **54**, 167 (1975).
37. T. B. Gatski, M. Y. Hussaini, and J. L. Lumley, *Simulation and Modeling of Turbulent Flows*, Oxford University Press, Oxford, U.K., 1996.
38. P. Moin and K. Mahesh, *Ann. Rev. Fluid Mech.* **30**, 539 (1998).
39. B. A. Galperin and S. A. Orszag, *Large Eddy Simulation of Complex Engineering and Geophysical Flows*, Cambridge University Press, Cambridge, U.K., 1993.
40. M. Lesieur and O. Métais, *Ann. Rev. Fluid Mech.* **28**, 45 (1996).
41. C. Meneveau and J. Katz, *Ann. Rev. Fluid Mech.* **32**, 1 (2000).
42. B. E. Launder and D. B. Spalding, *Lectures in Mathematical Models of Turbulence*, Academic Press, London, U.K., 1972.
43. D. C. Wilcox, *Turbulence Modeling for CFD*, DCW Industries, Inc., La Canada, Califo., 1993.
44. C. G. Speziale, *AIAA Journal* **36**, 173 (1998).
45. S. Tavoularis, *Measurement in Fluid Mechanics*, Cambridge University Press, Cambridge, U.K., (to be published).
46. R. P. Benedict, *Fundamentals of Temperature, Pressure and Flow Measurements*, 2nd ed., Wiley-Interscience, New York, 1977.
47. T. G. Beckwith, R. D. Marangoni, and J. H. Lienhard, *Mechanical Measurement* 5th ed., Addison-Wesley, Reading, Mass., 1993.
48. E. O. Doebelin, *Measurement Systems Application and Design*, 5th ed., McGraw-Hill, New York, 2004.
49. R. J. Emrich, ed., in L. Marton and C. Marton, eds., *"Fluid dynamics"* Methods of Experimental Physics, Vols. 18A and B. Academic Press, New York, 1981.
50. R. J. Goldstein, *Fluid Mechanics Measurements*, 2nd ed., Taylor and Francis, Washington, 1996.
51. F. Mayinger and O. Feldmann eds., *Optical Measurements*, 2nd ed., Springer, Berlin, 2001.
52. E. Ower and R. C. Pankhurst, *The Measurement of Air Flow*, Pergamon Press, Oxford, U.K., 1977.
53. T. Arts, et al., *Measurement Techniques in Fluid Dynamics*, 2nd ed., von Karman Institute for Fluid Dynamics, Rhode-Saint Genese, Belgium, 2001.
54. J. G. Webster, ed., *The Measurement, Instrumentation and Sensors Handbook*, CRC Press, Boca Raton, Flor., 1999.
55. S. Tavoularis, in N. P. Cheremisinoff, ed., *Techniques for turbulence measurement Encyclopedia of Fluid Mechanics*, Vol. 1, Chapter 36, Gulf Publishing Co., Houston, 1986, pp. 1207–1255.
56. J. S. Bendat and A. G. Piersol, *Random Data Analysis and Measurement Procedures*, 3rd ed., John Wiley & Sons, Inc., New York, 2000.

57. H. W. Coleman and W. G. Steele, *Experimentation and Uncertainty Analysis for Engineers*, 2nd ed., John Wiley & Sons, Inc., New York, 1999.
58. H. W. Coleman and W. G. Steele, in R. W. Johnson, ed., *"Uncertainty analysis"* The Handbook of Fluid Dynamics, CRC Press, Boca Raton, Flon., 1998, pp. 39.1–39.11.
59. R. C. Baker, *Flow Measurement Handbook*, Cambridge University Press, Cambridge, U.K., 2000.
60. R. A. Furness, *Fluid Flow Measurement*, Longman, London, U.K., 1989.
61. A. T. J. Hayward, *Flowmeters*, McMillan Press, London, 1979.
62. H. H. Bruun, *Hot-Wire Anemometry*, Oxford University Press, Oxford, U.K., 1995.
63. C. G. Lomas, *Fundamentals of Hot Wire Anemometry*, Cambridge University Press, Cambridge, U.K., 1986.
64. G. Comte-Bellot, *Ann. Rev. Fluid Mech.* **8**, 209 (1976).
65. R. J. Adrian, in R. J. Goldstein, ed., *"Laser velocimetry"* Fluid Mechanics Measurements, Taylor and Francis Publishers, Washington, 1996, pp. 175–299.
66. H.-E. Albrecht, M. Borys, N. Damaschke, and C. Tropea, *Laser Doppler and Phase Doppler Measurement Techniques*, Springer-Verlag, Berlin, 2003.
67. P. Buchhave, W. K. George, and J. L. Lumley, *Ann. Rev. Fluid Mech.* **11**, 443 (1979).
68. F. Durst, A. Melling, and J. H. Whitelaw, *Principles and Practice of Laser Doppler Anemometry*, Academic Press, New York, 1976.
69. M. Raffel, C. E. Willert, and J. Kompenhans, *Particle Image Velocimetry, A Practical Guide*, Springer, Berlin, 1998.
70. I. Grant, *Proc. Instn. Mech. Engrs. Part C* **211**, 55 (1997).
71. J. Westerweel, *Meas. Sci. Technol.* **8**, 1379 (1997).
72. J. C. Wyngaard, *Ann. Rev. Fluid Mech.* **13**, 399 (1981).
73. A. C. Eckbreth, *Laser Diagnostics for Combustion Temperature and Species*, 2nd ed., Gordon and Breach Publishers, Canada, 1996.
74. C. Mercer, ed., *Optical Metrology for Fluids, Combustion and Solids*, Kluwer Academic Publishers, Dordrecht, Netherlands, 2003.
75. W.-J. Yang, *Handbook of Flow Visualization*, Taylor and Francis, 1989.
76. W. Merzkirch, *Flow Visualization*, 2nd ed., Academic Press, New York, 1987.
77. A. J. Smits and T. T. Lim, eds., *Flow Visualization Techniques and Examples*, Imperial College Press, London, U.K., 2000.
78. Japan Society of Mechanical Engineers, *Visualized Flow*, Pergamon Press, Oxford, U.K., 1988.
79. G. S. Settles, *Schlieren and Shadowgraph Techniques*, Springer, Berlin, 2001.

STAVROS TAVOULARIS
University of Ottawa